JNC TN9400 2004-043

SIMMER-III Structure Model

- Model and Method Description -

(Research Document)

July, 2004

O-arai Engineering Center

Japan Nuclear Cycle Development Institute

〒319-1184　茨城県那珂郡東海村村松４番地４９
核燃料サイクル開発機構
技術展開部　技術協力課
電話：029-282-1122（代表）
ファックス：029-282-7980
電子メール：jserv@jnc.go.jp

Ⓦ

JNC TN9400 2004-043
July, 2004

SIMMER-III Structure Model

- Model and Method Description -

(Research Document)

Kenji Kamiyama* and Satoru Kondo**

Abstract

An advanced safety analysis code, SIMMER-III has been developed to evaluate the consequence of postulated core disruptive accidents of liquid-metal fast reactors (LMFRs). The present report describes a structure model for SIMMER-III to analyze a disrupting core.

The structure in SIMMER-III, consisting of fuel pins and subassembly can walls, is modeled to exchange heat and mass with multiphase multicomponent flow of disrupted core material and to provide flow channel for fluids. In addition, complex behavior is modeled which changes configurations of structures as a result of heat and mass transfer from molten core materials.

The structure model described in the present report alleviates some of limitations in the previous code SIMMER-II, and hence it is expected that the future researches with SIMMER-III will significantly improve the reliability and accuracy of LMFR safety analysis.

* Nuclear System Safety Research Group, Advanced Technology Division, O-arai Engineering Center, JNC

** Office of Planning and Arrangement for New Organization, Head Quarters JNC

JNC TN9400 2004-043
2004 年 7 月

SIMMER-III 構造材モデル

―モデルおよび手法の記述―

（研究報告）

神山　健司*、近藤　悟**

要　　旨

SIMMER-III コードは、液体金属冷却高速炉の炉心崩壊事故の影響を評価するため開発されてきた。本報告書では、崩壊する炉心を解析するための SIMMER-III 構造材モデルを記述する。

SIMMER-III の構造材は、集合体ラッパ管および燃料ピンといった固体構造にて構成され、崩壊炉心物質の多相・多成分流と熱および質量移行を行なうとともに、流体へ流路を与えるようモデル化されている。加えて、溶融炉心物質からの熱および質量移行の結果として、構造材の形状が変化する複雑な挙動もモデル化されている。

本報告書に記述される構造材モデルによって先行コード SIMMER-II に見られた構造材のモデル化に関する種々の限界が改善され、SIMMER-III コードを用いた高速炉の安全解析の信頼性および精度の向上が期待される。

*　大洗工学センター　要素技術開発部　リスク評価研究グループ
** 本社　新法人設立準備室

Contents

List of Tables

List of Figures

Nomenclature

a : Interface area per unit volume [1/m]

c : Heat capacity [J/kg/K]

C_{GAP} : The surface roughness of the fuel pellet and the cladding

D_h : Hydraulic diameter [m]

e : Specific internal energy [J/kg]

$e_{sol,M}$: Solidus energy for material M [J/kg]

$e_{liq,M}$: Liquidus energy for material M [J/kg]

$h_{f,M}$: Latent heat of fusion for material M [J/kg]

h : Heat transfer coefficient [W/m^2/K]

h_{GAP} : Heat transfer coefficient between the fuel pin and the cladding [W/m^2/K]

m : Mass [kg]

P_m : Power amplitude

P_{GAP} : Pressure of the gap between the fuel pellet and the cladding [Pa]

Q_{hc} : Rate of energy interchange between fluid and cladding [W]

Q_{hb} : Rate of energy interchange between fluid and fuel pellet surface [W]

Q_{Hm} : Energy transfer rates due to heat transfer from fluid [W]

Q_{Nm} : Energy transfer rates due to f nuclear heating [W]

R_5 : Gas constant of fission gas

r_{C0} : Radius of left cell boundary in the cylindrical geometry [m]

r_{C1} : Radius of right cell boundary in the cylindrical geometry [m]

r_m : Radius of the boundary for can wall and crust components [m], (m=1 - 6)

r_{tm} : Radius of temperature point for can wall and crust components [m], (m=1 - 6)

r_{pm} : Radius of the boundary and temperature point for the fuel pin components [m], (m=1 – 6)

T : Temperature [K]

V : Cell volume [m^3]

v : Specific volume [m^3/kg]

W : Thickness of can wall [m]

w_5 : The molecular weight of fission gas [kg]

Greek letters

α : Volume fraction

δ : Thermal penetration length [m]

Δt : Time step [s]

ΔR : Mesh cell width [m]

ε : Emissivity

κ : Thermal Conductivity [W/m/K]

Γ_c : Mass-transfer per unit volume to the cladding [kg/s/m^3]

Γ_m : Mass-transfer per unit volume to the component m [kg/s/m^3]

$\overline{\rho}$: Macroscopic density [kg/m^3]

ρ : Density [kg/m^3]

σ_{SB} : Stefan-Boltzmann constant (5.67×10^{-8} W/m^2/K^4)

$\tau_{str,M}$: Structure time constant [s]

Subscripts

a : Fuel pin interior node

b : Fuel pin surface node

c : Cladding

CF : Crust fue

cnt : Control

f : Fuel

FG : Fission gas

gas : Gas

g_m : Density components of gas (m=1-5), see Table 2-3.

G_m : Material components of gas (m=1-4), see Table 2-3.

int : Fuel pin interior node

LCW : Left can wall

lm : Density components of liquid (m=1-13), see Table 2-2.

Lm : Energy components of liquid (m=1-7), see Table 2-2.

M : Material component

$M_1 = 1$: Fuel

$M_1 = 2$: Steel

max : Maximum value

min : Minimum value

nf : Non-flow volume

pin : Fuel pin

rad : Radiation heat transfer

RCW : Right can wall

s : Steel

sm : Density components of structure (m=1-12), see Table 2-1.

Sm : Energy components of structure (m=1-9), see Table 2-1.

Superscripts

0 : Zero (minimum) value

EQ : Equilibrium mass transfer

i : Input variable

n : Initial value of time step *n*

~ $n+1$:Updated value in time step *n*

1. Introduction

SIMMER-III has been developed to evaluate the consequence of postulated core disruptive accidents (CDAs) of liquid-metal fast reactors (LMFRs). Although the extensive safety design effort for accident prevention has made the occurrence of such an event extremely unlikely, the importance of CDAs is still emphasized from the viewpoint of safety design and evaluation to appropriately mitigate and accommodate the consequences and thereby to minimize the risk to the public. A recriticality and resultant energetics potential during the so-called transition phase of CDAs is regarded as one of the most important risk contributors. Complexities of evaluating the transition phase, together with limited experimental data in comparison with the initiating phase of CDAs, tend to introduce relatively large uncertainties into the safety analyses in the past [1, 2].

SIMMER-III has been developed to alleviate some of limitations in the previous SIMMER-II code [3, 4] and thereby to provide a next-generation tool for more reliable analysis of the transition phase. SIMMER-III is a two-dimensional, three-velocity-field, multiphase, multicomponent, Eulerian, fluid-dynamics code coupled with a space- and energy-dependent neutron kinetics model. The conceptual overall framework of the code is shown in Fig. 1-1. The entire code consists of three elements: the fluid-dynamics model, the structure model, and the neutronics model. The fluid-dynamics portion, which constitutes about two thirds of the code, is interfaced with the structure model through heat and mass transfer at structure surfaces. The neutronics portion provides nuclear heat sources based on the mass and energy distributions calculated by the other code elements.

The structure field in SIMMER-III represents solid components consisting of fuel pins and subassembly can walls. The structure exchanges heat and mass with multiphase multicomponent flow and provides a flow channel for fluid. In addition, SIMMER-III ought to model the remaining solid structures together with their disintegration behavior since the code is primarily intended for evaluation of a disrupted reactor core state. Therefore sufficiently detailed and flexible modeling is desired to reasonably simulate the core melt-out behavior during CDAs, and consequently the can wall model has been significantly improved over the previous SIMMER-II as described in Section 2.1. On the other hand, the accident progression behavior in a core

disruption stage of CDAs is less sensitive to modeling details of fuel pins, especially for a loss-of-flow accident. This is in contrast with the CDA's initiation phase in which accident progression is sensitive to fuel-pin mechanics as modeled in SAS-series codes [5]. For this reason, a simplified fuel-pin model has been firstly developed for SIMMER-III as a standard model. This simplified modeling, however, has some deficiencies under such the situation as a transient over power accident in which fuel motion inside the cladding has relatively large effects on the sequence of CDAs. Therefore, for a better simulation of fuel pin behavior during such a transient, the current SIMMER-III code (Version 3.A) [6] finally contains an optional detailed fuel-pin model consisting of finer radial heat transfer of in-pin fuel, molten cavity formation, cladding mechanical failure, molten fuel ejection and in-pin fuel motion. A simple model for plenum fission gas blow-down is also implemented into the current version. Since provision of the detailed pin model description will be made in the near future, the simplified pin model is mainly described in the present report.

The development of the SIMMER-III code has reached a stage, where all the models originally intended are made available, and integral calculations with the code can be made. In parallel to the code development, an extensive program has been performed for systematic and comprehensive code assessment under the collaboration with Forschungszentrum Karlsruhe (FZK), Germany, Commissariat à l'Energie Atomique (CEA) and Institute for Radioprotection and Nuclear Safety (IRSN) France [7]. Furthermore, in order to solve the numerical limitation of dimensionality of SIMMER-III, the Japan Nuclear Cycle Development Institute (JNC) is developing a three-dimensional code SIMMER-IV [8]. The basic policy of SIMMER-IV is a direct extension of SIMMER-III to three dimensions with retaining exactly the same framework in physical models as SIMMER-III. Since each fluid-dynamics mesh cell is coupled with six neighboring cells in SIMMER-IV, the can walls are placed on four mesh cell boundaries which are front and back in addition to left and right in SIMMER-III. The treatment of the additional front and back can walls is identical with the left and right can walls in SIMMER-III.

Hence, the present report describes the modeling of the core structure employed in Version 3.A of SIMMER-III. In the rest of this report, the overview of the model of SIMMER-III is concisely described in Chapter 2. In Chapter 3, the input and

initialization both of the fuel pin and the can wall are described. Chapter 4 explains the structure configuration model which is a key method of the SIMMER-III structure model. The heat-transfer model for the can wall and the fuel pin are described in Chapter 5 and 6, respectively. In Chapter 7, the structure breakup models are described.

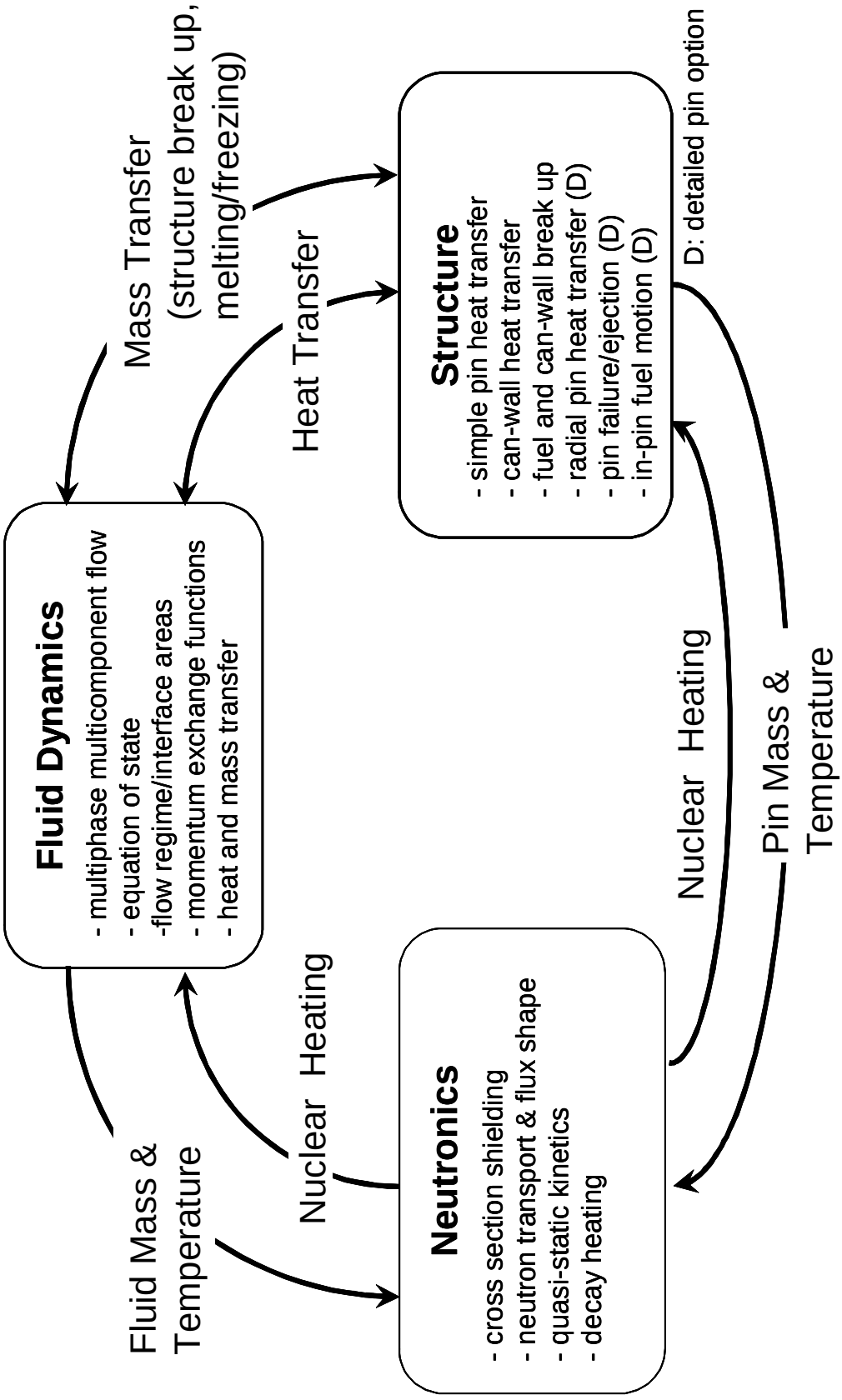

Fig. 1-1 SIMMER-III Overall Code Structure.

2. Overview of the Structure Model

In this Chapter, the features of the structure model are described briefly in comparison with SIMMER-II in order to clarify the scope of model development. In order to facilitate an understanding of model and method description, the definition of components used throughout SIMMER-III is shown in this Chapter. In addition, the assumptions employed in the model are described in order to define the scope of the code application.

2.1. Improvement from Previous Code SIMMER-II

The can wall model has been improved in two major aspects. First two can walls, assumed to be present at radial mesh cell boundaries, are now distinguished between left and right boundaries. Crust fuel resulted from freezing of liquid fuel on can wall surface is also distinguished. This treatment increased the number of structure-field components and is not desirable for efficiency of calculation, but it is very advantageous to better simulate the core melt-out behavior in CDAs and flexibly represent the structure walls in the experimental analysis. Second the can wall heat-transfer calculation was advanced by representing a can wall by two temperature nodes: the surface node closely coupled with fluid and the interior node.

The standard fuel-pin model is simple but still improved from SIMMER-II by representing the pellet fuel by two nodes and by allowing simulate the gap thermal resistance. Furthermore, the detailed pin model was introduced to accurately simulate fuel-pin behavior in some of CDA sequence.

The structure breakup model is also made much more flexible than SIMMER-II as described in Chapter 7. The intra- and inter-granular fission gas components in the pin fuel are not distinguished in SIMMER-III, because such detailed treatment is judged to be beyond the scope of this code. Improvement exists, however, in the modeling of fission gas in the liquid-field fuel components and this eliminates a problem of instantaneous release and unphysical pressurization observed in SIMMER-II.

2.2. SIMMER-III Components

The list of structure components is shown in Table 2-1, which is useful to help follow all of the model descriptions. In addition, the list of liquid and vapor components are also shown in Table 2-2 and Table 2-3 respectively, which is also useful to help follow the

model described mainly in Chapter 7. In these tables, the lower-case subscripts denote density components while the upper-case subscripts denote energy components commonly used throughout SIMMER-III. The fuel components are divided into fertile and fissile in their mass (density components) to represent different enrichment zone in the core. However, the two materials are assumed to be mixed intimately, and hence the single temperature is assigned as an energy component. Namely, for example for the pin fuel surface node, the volume fraction, which is used as the energy component, is represented by

$$\alpha_{S1} = (\overline{\rho}_{s1} + \overline{\rho}_{s2})v_{S1} \quad , \tag{2-1}$$

where v_M is the component specific volume used in the SIMMER-III EOS model [9, 10].

The pin interior component is not included in Table 2-1, because it is treated only in the fuel pin model. The pin interior is modeled by one-point temperature node in a standard simple model. The pin related components are listed in Table 2-4.

2.3. Fuel Pin Geometry and Assumptions

The axial geometry of the simplified fuel-pin model is shown in Fig. 2-1, which simulate a typical LMFR fuel pin structure. The upper and lower axial blanket regions and upper and lower fission-gas plenum regions can be placed above and below the active core fuel zone. The same configuration can be used for a control pin, as well, but two types of pins cannot co-exist in a same mesh cell.

The radial fuel-pin geometry is shown in Fig. 2-2. The pin fuel is modeled by two temperature nodes, while the thin cladding is represented by one node. The surface pin fuel node has a thickness of thermal penetration length, calculated by an input structure thermal time constant represented in the later Section 3.2. The temperature point of the pin fuel interior is placed at the volume centroid. The cladding, or the pin fuel surface node when cladding is missing, undergoes heat and mass transfer with fluid, whereas the pin fuel interior is not directly coupled with fluid.

Other assumptions with respect to the simplified pin model are summarized below:

(1) The thermal calculation of the fuel pin is performed outside the fluid-dynamics calculation and is operated at a different time step control. Because of the close relation between nuclear heating and fuel thermal

response, the fuel-pin heat-transfer time steps are operated at the same control as reactivity steps. However, an option is available to force the heat-transfer time steps to be identical to fluid time steps.

(2) In the simplified pin model, there is no explicit treatment of a central hole or a fuel-cladding gap. The former volume can be included by specifying the porosity of pin fuel, and latter volume by a non-flow volume. The non-flow volume is made available to flow when the cladding failure is predicted.

(3) The gap conductance is included in the heat-transfer coefficient between pin-fuel surface and cladding.

(4) The pin-fuel interior node is decoupled with fluid-dynamics models because of its large thermal inertia and slow response to change in fluid condition.

(5) No mass transfer from pin fuel surface to fluid is modeled, since the possibility of surface melting in LMFR accident is unlikely or less important.

(6) No crust fuel can be placed on a cladding surface, since the cladding ablation should occur first rather than fuel freezing especially under high-temperature condition of LMFR accidents.

(7) A control pin is modeled similarly to the fuel pin.

(8) Fission gas plena can be placed both at the upper and lower regions of the pin. The fission gas existing over several axial mesh cells is assumed to be at uniform temperature.

(9) Currently structure breakup or pin failure (pin fuel and cladding) is based on thermal criteria mainly. The mass and energy are transferred to liquid and particle components depending on the melt fractions of components being transferred.

(10) No fission gas release is modeled directly from pin fuel, but the fission gas in pin fuel is transferred to liquid and particle/chunk fuel upon fuel breakup and later release from these liquid-field fuel components is modeled.

(11) The fuel-pin heat-transfer calculation is based on internal energies to be

consistent with fluid dynamics. Pin-fuel temperature is calculated implicitly, while fission gas temperature is updated explicitly because of slow thermal response of gas.

It should be noted that recently there are some studies to apply the SIMMER-III/IV code to various types of reactors, although the code is primarily developed to evaluate sequences and consequences of the transition phase of CDAs. An application to the gas-cooled reactors is one of example, and various types of fuel assembly, a block-type fuel for example, are being proposed in the design study of that reactor. Therefore, as an optional block-type fuel compact model was implemented into the current version of SIMMER in order to evaluate the steady-state phase and transient sequences. In this fuel concept, the coolant gas flows through graphite matrix containing a lot of coated particles. The optionally introduced model simply regards the fuel assembly as a cylinder of each component; i.e. inner cylinder for gas coolant, medium cylinder for matrix and outer cylinder for fuel. It should be noted that, in this model, a pin outer radius defined in the simplified pin model is regarded as a thickness of the fuel and matrix. A new input parameter RCOMPB specifies an outer radius of the fuel compact assembly. The heat transfer calculation in this compact fuel model is made in the same way as in the standard pin model except for the different location of each component.

2.4. Can Wall Geometry and Assumptions

The radial can wall geometry over three successive mesh cells, ij-1, ij and ij+1, is shown in Fig. 2-3. Each can wall is represented by two nodes, the surface and interior, and the temperatures are calculated at the volume centroid of the nodes. The thickness of a surface node is determined from an input-specified thermal penetration length of steel represented in the later Section 3.2 and roughly corresponds to 1/10 of a total can wall thickness. In the standard option, the can wall is represented by a slab geometry to simulate the hexagonal subassembly wrapper tubes. An option is also available to model the can wall by a cylindrical geometry to simulate, for example, a tube wall in some experimental analysis.

At each mesh cell boundary, two can walls can be placed at the same time, together with the non-flow volumes in-between, to simulate inter-subassembly gaps in a reactor. Only one non-flow volume is actually meaningful, but both the left and right volumes can be specified just for flexibility. A normal can wall is regarded as “thick” and is

modeled by the surface and interior nodes. When the wall becomes “thin”, the wall can no longer be modeled by two nodes and is represented by a single interior node.

For fluid flows, the can wall structure provides a channel wall for an axial flow, and no radial flow across the cell boundary is permitted as long as one of two can walls is present. The can walls exchange heat and mass with fluid in a mesh cell, and no inter-cell heat transfer is permitted when two walls are present at the cell boundary. However, when one of the two can walls becomes missing, then inter-cell heat transfer is calculated. This is done by setting a fraction of the interior node to be a surface node over in an adjacent cell. For example, let us consider the right boundary of a cell ij, where a thick right can wall is present and left can wall in cell ij+1 is missing. Three can wall nodes, $S7$ and $S8$ in cell ij, and $S5$ in cell ij+1, are defined in this case. The surface node in cell ij, $S7$, undergoes heat and mass transfer with fluid in cell ij, while the surface node in cell ij+1, $S5$, undergoes heat and mass transfer with fluid in cell ij+1. The three can wall nodes are coupled in the structure heat-transfer calculations.

Other assumptions with respect to the can-wall structure model are summarized below:

(1) The thermal calculation of the can walls is performed within the fluid-dynamics calculation and is operated at the same time step control.

(2) When two walls are present at a cell boundary, two mesh cells are thermally decoupled. The boundary condition outside the interior node is adiabatic.

(3) Non-flow volumes can be specified for simulating inter-subassembly gaps, but the presence of liquid sodium in the gaps is ignored. No thermal resistance of the gap is considered. The non-flow volume is made available to flow upon failure of the can wall.

(4) The fuel crust can be placed on both the left and right can wall surfaces and they are distinguished each other.

(5) The heat transfer calculation of the can wall and fuel crust is performed in up to five temperature nodes. Based on internal energies to be consistent with fluid dynamics, heat transfers are calculated implicitly.

(6) Currently structure breakup of the fuel crust and the can walls is modeled, mainly based on thermal criteria. Additional breakup mechanisms are also implemented as described in the later sections.

Table 2-1 SIMMER-III Fluid Dynamics Structure Field Components.

Density Components (MCSR)		Energy Components (MCSRE)	
*s*1	Fertile Pin Fuel Surface Node	*S*1	Pin Fuel Surface Node
*s*2	Fissile Pin Fuel Surface Node		
*s*3	Left Fertile Fuel Crust	*S*2	Left Fuel Crust
*s*4	Left Fissile Fuel Crust		
*s*5	Right Fertile Fuel Crust	*S*3	Right Fuel Crust
*s*6	Right Fissile Fuel Crust		
*s*7	Cladding	*S*4	Cladding
*s*8	Left Can Wall Surface Node	*S*5	Left Can Wall Surface Node
*s*9	Left Can Wall Interior Node	*S*6	Left Can Wall Interior Node
*s*10	Right Can Wall Surface Node	*S*7	Right Can Wall Surface Node
*s*11	Right Can Wall Interior Node	*S*8	Right Can Wall Interior Node
*s*12	Pin Control Surface Node	*S*9	Pin Control Surface Node

Table 2-2 SIMMER-III Fluid Dynamics Liquid Field Components.

Density Components (MCLR)		Energy Components (MCLRE)	
*l*1	Liquid Fertile Fuel	*L*1	Liquid Fuel
*l*2	Liquid Fissile Fuel		
*l*3	Liquid Steel	*L*2	Liquid Steel
*l*4	Liquid Sodium	*L*3	Liquid Sodium
*l*5	Fertile Fuel Particles	*L*4	Fuel Particles
*l*6	Fissile Fuel Particles		
*l*7	Steel Particles	*L*5	Steel Particles
*l*8	Control Particles	*L*6	Control Particles
*l*9	Fertile Fuel Chunks	*L*7	Fuel Chunks
*l*10	Fissile Fuel Chunks		
*l*11	Fission Gas in Liquid Fuel		
*l*12	Fission Gas in Fuel Particles		
*l*13	Fission Gas in Fuel Chunks		

Table 2-3 SIMMER-III Fluid Dynamics Vapor Field Components.

Density Components (MCGR)		Material Components (MCGM1)	
$g1$	Fertile Fuel vapor	$G1$	Fuel Vapor
$g2$	Fissile Fuel vapor		
$g3$	Steel Vapor	$G2$	Steel Vapor
$g4$	Sodium Vapor	$G3$	Sodium Vapor
$g5$	Fission gas	$G4$	Fission gas

Table 2-4 SIMMER-III Fuel-Pin Components

Simple Model (standard)	
a	Pin Fuel or Control Interior Node
b	Pin Fuel or Control Surface Node (=S1 or S9)
c	Cladding (=S4)
	Fission Gas in Pin Fuel

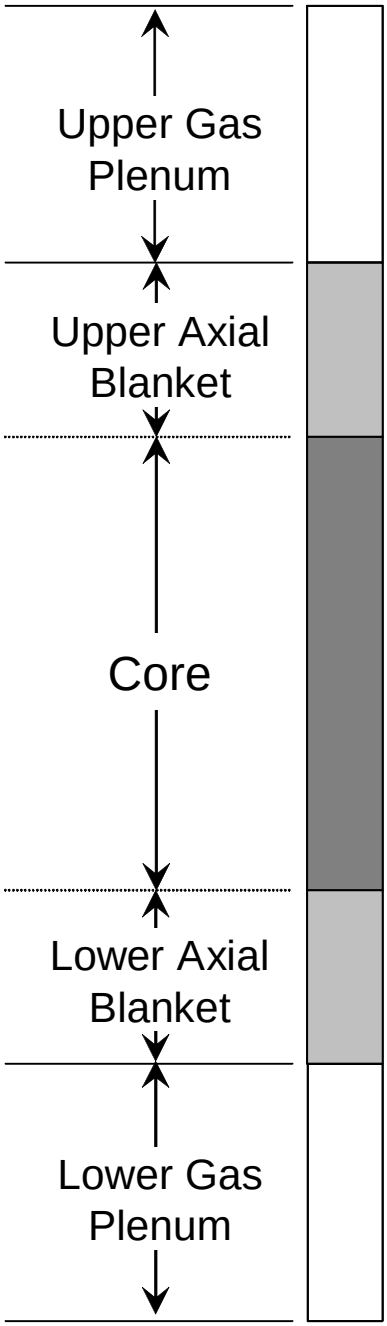

Fig. 2-1 Axial Fuel Pin Representation in SIMMER-III (Simple Model)

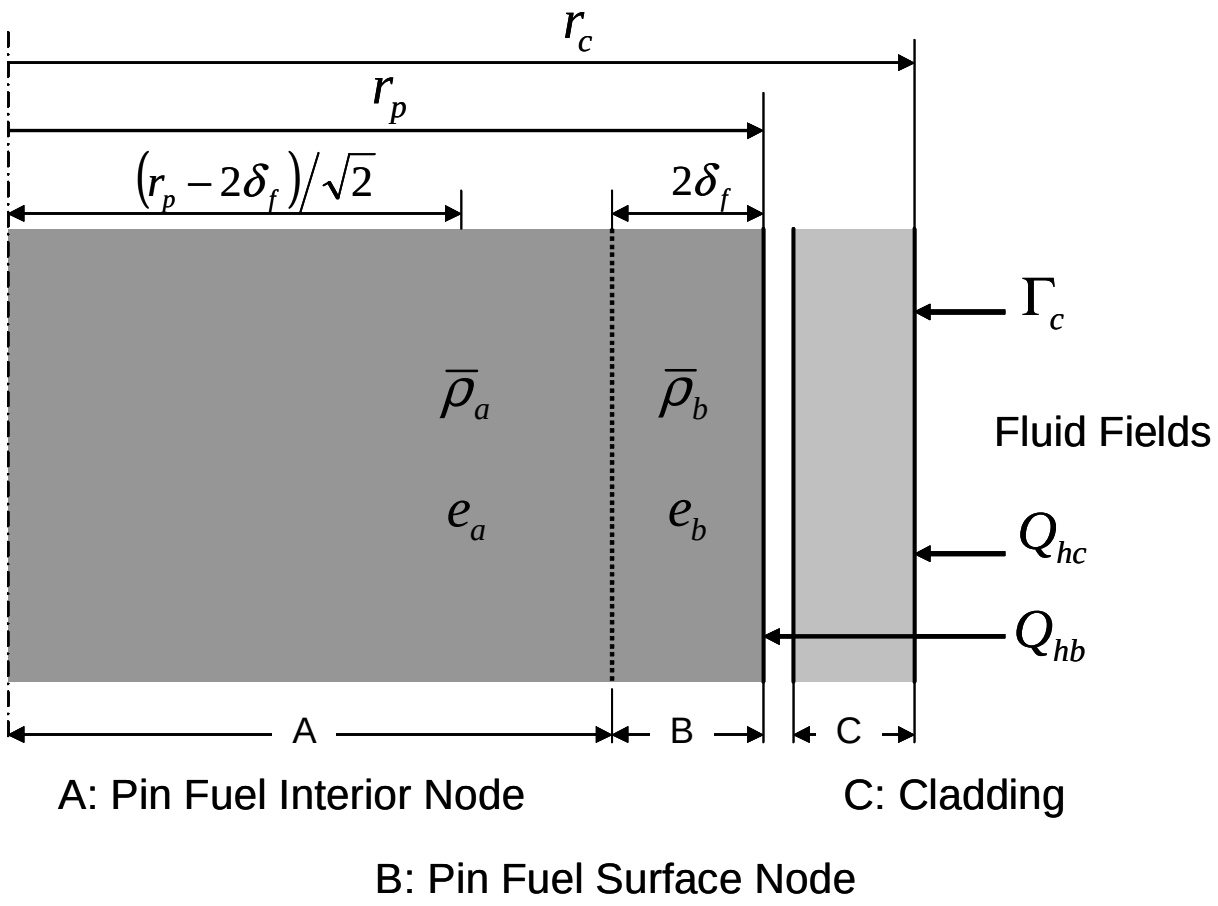

Fig. 2-2 Radial Fuel Pin Cross Sections in SIMMER-III (Simple Model).

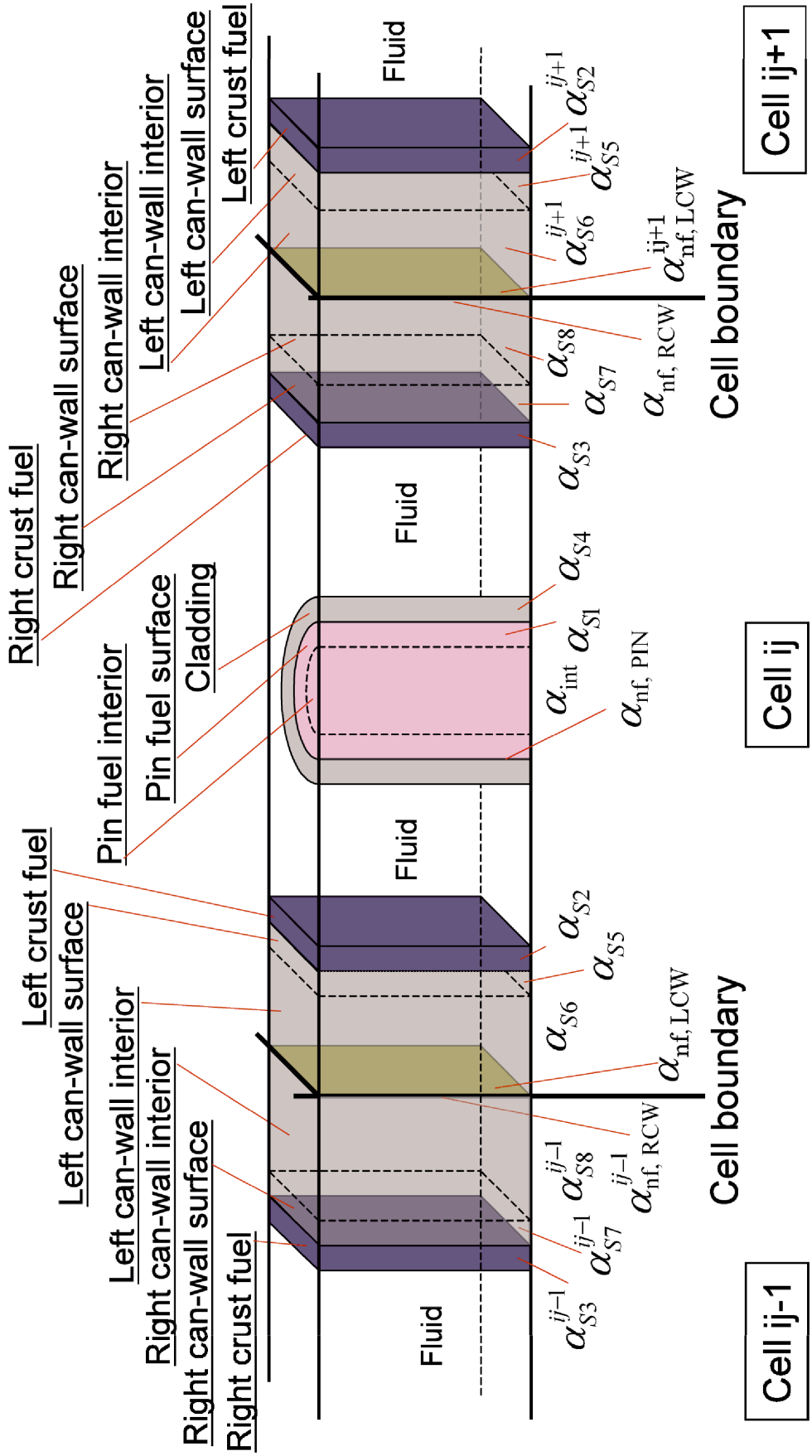

Fig. 2-3 Fuel Pin and Can Wall Configuration in a Mesh Cell.

3. Input Data and Initialization

3.1. Input Specification

Masses and energies of structure-field energy components are specified, similarly to other SIMMER-III components, by initial volume fractions and temperatures. They are then converted, by calling the equation-of-state (EOS) functions [9, 10] during initialization process, to macroscopic densities and specific internal energies, which are the independent variables in SIMMER-III. Partition of fuel mass into fertile and fissile density components is based on input fissile enrichments.

The following input variables are used for setting up the initial conditions for the SIMMER-III structure field.

(1) Structure thermal time constants for fuel and steel.

(2) Initial volume fractions of structure-field components.

(3) Initial temperatures of structure-field components.

(4) An initial fuel-pin radius defined as the cladding outer radius.

(5) Initial surface areas per unit volume for cladding, left and right can walls.

(6) Axial geometry of fuel pin.

(7) Plenum fission gas pressure and temperature (upper and lower).

It should be noted that the input of the initial surface areas for can walls are not necessary in the cylindrical can wall model, because they are automatically defined in the initialization process depending on the volume fractions of walls and radii of cell boundaries.

3.2. Thermal Penetration Lengths

The thicknesses of pin fuel and can wall surface nodes are defined as the thermal penetration lengths, $2\delta_M$, considering the transient thermal response of the surface nodes. They are determined from the input structure time constants specified for fuel and steel, as follows:

$$2\delta_M = \psi\sqrt{\kappa_M \tau_{str,M} / \rho_M c_M} \qquad (3\text{-}1)$$

where κ_M , ρ_M and c_M are thermal conductivity, density and heat capacity, respectively, of material M (1 for fuel and 2 for steel). These properties are evaluated by the EOS functions with assuming the solidus energies. The input structure time constants are specified by input. The thermal penetration lengths are calculated only once in the code during initialization and stay constant during the transient calculation. Thus the selection of $\tau_{str,M}$ should be made considering the time scale of the problem being calculated. The proportional constant ψ is defined in SIMMER-III as

$$\psi = 2\sqrt{3}\,, \tag{3-2}$$

where it is assumed that the transient temperature profile is approximated by a parabola.

Another factor in selecting the structure time constants is consideration of the stability of heat-transfer calculation. The structure-side heat-transfer coefficient of the surface node must be limited such that the heat transferred in a time step does not exceeds the enthalpy of the cell as expressed by

$$h = \kappa_M / \delta_M \le \overline{\rho}_M c_M / a_M \, \Delta t\,, \tag{3-3}$$

where $\overline{\rho}_M$ and a_M are the macroscopic density and heat-transfer area per unit volume, respectively, of the surface node. At the same time, the thermal penetration length is correlated with $\overline{\rho}_M$ and a_M as

$$2\delta_M = \overline{\rho}_M / (\rho_M a_M)\,. \tag{3-4}$$

By manipulating Eqs. (3-1) to (3-4), it is easy to show

$$\Delta t \le 6\tau_{str,M}\,. \tag{3-5}$$

The thermal time constant is normally set to a value much larger than the heat-transfer time step size, and hence there is no stability problem predicted. In other words, a limiter to the heat-transfer coefficient is inactive in most cases. However, care must be taken when one specifies an extremely small value for $\tau_{str,M}$ to simulate the case with extremely fast thermal response of the surface node under highly transient condition.

3.3. Fuel Pin Initialization

The fuel pellet radius is calculated, from the input initial pin radius, initial cladding volume fraction and initial pin surface area per unit volume, as

$$r_{pel} = r_{pin}^{i} \sqrt{\frac{\alpha_{\mathrm{int}}^{i} + \alpha_{S1}^{i}}{\alpha_{\mathrm{int}}^{i} + \alpha_{S1}^{i} + \alpha_{nf,PIN}^{i} + \alpha_{S4}^{i}}} \quad . \tag{3-6}$$

where the superscript i denotes the input variable. The thermal penetration length of fuel is restricted by the pellet radius as

$$2\delta_f = \min\left(2\delta_f , r_{pel}\right) \quad . \tag{3-7}$$

This means that the pin fuel can be represented only by the surface node, by specifying the large $\tau_{str,f}$ value. The volume fractions of two pin fuel nodes are rezoned based on the surface node thickness and are defined by

$$\alpha_{S1} = \frac{r_{pel}^2 - \left(r_{pel} - 2\delta_f\right)^2}{r_{pel}^2}\left(\alpha_{S1}^{i} + \alpha_{\mathrm{int}}^{i}\right) \text{ , and} \tag{3-8}$$

$$\alpha_{\mathrm{int}} = \left(\alpha_{S1}^{i} + \alpha_{\mathrm{int}}^{i}\right) - \alpha_{S1} . \tag{3-9}$$

where the subscripts $S1$ and int denote surface and interior pin fuel, respectively. The pin fuel temperatures are simply averaged as

$$T_{S1} = \begin{cases} T_{S1}^{i} & if \quad \alpha_{S1} < \alpha_{S1}^{i} \\ \dfrac{T_{S1}^{i}\alpha_{S1}^{i} + T_{\mathrm{int}}^{i}\left(\alpha_{S1} - \alpha_{S1}^{i}\right)}{\alpha_{S1}} & if \quad \alpha_{S1} \geq \alpha_{S1}^{i} \end{cases} \text{ , and} \tag{3-10}$$

$$T_{\mathrm{int}} = \begin{cases} T_{S1}^{i} & if \quad \alpha_{S1} < \alpha_{S1}^{i} \\ \dfrac{T_{\mathrm{int}}^{i}\alpha_{\mathrm{int}}^{i} + T_{S1}^{i}\left(\alpha_{\mathrm{int}} - \alpha_{\mathrm{int}}^{i}\right)}{\alpha_{\mathrm{int}}} & if \quad \alpha_{\mathrm{int}} < \alpha_{\mathrm{int}}^{i} \\ T_{\mathrm{int}}^{i} & if \quad \alpha_{\mathrm{int}} \geq \alpha_{\mathrm{int}}^{i} \end{cases} \quad . \tag{3-11}$$

Since material specific volumes are temperature-dependent variables in the SIMMER-III EOS model, the above procedure cannot conserve fuel mass. Therefore if

one tries to exactly conserve the initial fuel mass, the initial volume fractions for surface and interior pin fuel must be specified exactly by pre-evaluating the thermal penetration lengths $2\delta_f$.

The volume fractions and temperatures are then converted into the macroscopic densities and specific internal energies through EOS call. Then macroscopic density of fission gas in pin fuel is initialized by input specification, defined as the mass ratio to the pin fuel. Finally the fuel macroscopic densities for energy components are partitioned to fertile and fissile density components by input enrichment.

3.4. Fission-Gas Plenum Initialization

The fission gas plena can be placed both above and below the pin fuel column. The volume of a plenum is defined by the input pin non-flow volume, $\alpha_{nf,PIN}$. Based on input gas temperature and pressure, the microscopic density of plenum fission gas is calculated from the ideal-gas EOS,

$$\rho_{FG} = P_{FG}^{i} / \left(R_5 T_{FG}^{i} \right) \ , \tag{3-12}$$

where R_5 is the gas constant of fission gas. The total mass of fission gas is calculated by

$$m_{FG} = \rho_{FG} \sum_{j} \alpha_{nf,PIN} \ . \tag{3-13}$$

The specific internal energy of fission gas is calculated by EOS from the initial temperature.

3.5. Can Wall Initialization

The procedure to initialize the can wall components is essentially the same as fuel pin. Both the left and right can walls are treated in the same way, so only the left can wall is described below. There are some differences between the slab geometry and the cylindrical geometry when volume fractions are initialized.

First the thickness of a can wall is evaluated as

$$W_{LCW} = \frac{\alpha_{S5}^{i} + \alpha_{S6}^{i}}{a_{LCW}^{i}} \quad \text{for the slab geometry and,} \tag{3-14}$$

$$W_{LCW} = \sqrt{r_{C0}^2 + \left(r_{C1}^2 - r_{C0}^2\right)\left(\alpha_{S5}^i + \alpha_{S6}^i\right)} - r_{C0}^2 \quad \text{for the cylindrical geometry,} \tag{3-15}$$

where r_{C0} and r_{C1} are radii of the left and right boundary respectively of cell ij.

If $W_{LCW} < 4\delta_s$, the can wall is regarded as a thin wall and all the can wall volume fraction is represented by the interior node. The can wall initial variables of volume fraction and temperature are calculated respectively by

$$\alpha_{S5} = 0\,,\ \alpha_{S6} = \alpha_{S5}^i + \alpha_{S6}^i\,, \tag{3-16}$$

$$T_{S5} = T_s^0\,, \text{ and} \tag{3-17}$$

$$T_{S6} = \frac{\alpha_{S5}^i T_{S5}^i + \alpha_{S6}^i T_{S6}^i}{\alpha_{S6}}\ , \tag{3-18}$$

where T_s^0 is the zero temperature defined by the minimum internal energy in EOS.

If $W_{LCW} \geq 4\delta_s$, the can wall is regarded as a thick wall and two temperature nodes are defined. The volume fractions of two can wall nodes are rezoned based on the surface node thickness. For the slab geometry, they are defined by

$$\alpha_{S5} = 2\delta_S a_{LCW}^i\,, \text{ and} \tag{3-19}$$

$$.\,\alpha_{S6} = \left(\alpha_{S5}^i + \alpha_{S6}^i\right) - \alpha_{S5} \tag{3-20}$$

For the cylindrical geometry, they are defined by

$$r_{S5} = \sqrt{r_{C0}^2 + \left(r_{C1}^2 - r_{C0}^2\right)\left(\alpha_{S5}^i + \alpha_{S6}^i\right)}\,,\ r_{S6} = r_{S5} - 2\delta_s\,, \tag{3-21}$$

$$\alpha_{S5} = \frac{r_{S5}^2 - r_{S6}^2}{r_{C1}^2 - r_{C0}^2}\,, \text{ and} \tag{3-22}$$

$$\alpha_{S6} = \frac{r_{S6}^2 - r_{S0}^2}{r_{C1}^2 - r_{C0}^2}\,. \tag{3-23}$$

Then the can wall initial temperatures are simply averaged as

$$T_{S5} = \begin{cases} T_{S5}^{i} & if \quad \alpha_{S5} < \alpha_{S5}^{i} \\ \dfrac{T_{S5}^{i}\alpha_{S5}^{i} + T_{S6}^{i}\left(\alpha_{S6} - \alpha_{S6}^{i}\right)}{\alpha_{S5}} & if \quad \alpha_{S5} \geq \alpha_{S5}^{i} \end{cases}, \text{ and} \tag{3-24}$$

$$T_{S6} = \begin{cases} \dfrac{T_{S6}^{i}\alpha_{S6}^{i} + T_{S5}^{i}\left(\alpha_{S6} - \alpha_{S6}^{i}\right)}{\alpha_{S6}} & if \quad \alpha_{S6} < \alpha_{S6}^{i} \\ T_{S6}^{i} & if \quad \alpha_{S6} \leq \alpha_{S6}^{i} \end{cases}. \tag{3-25}$$

4. Structure Configuration Model

4.1. Overview of Structure Configuration Model

During a SIMMER-III transient calculation, the state and configuration of the structure components change with time, through various modes of heat and mass exchange with fluid. When a certain condition is satisfied, the structure component breaks up and its mass is transferred to the corresponding fluid components. The structure configuration model of SIMMER-III performs the following operations:

(1) Identify the presence to structure components;

(2) Determine the structure surface components that directly interact with fluid;

(3) Re-zone the surface nodes of pin fuel and can walls and calculate radial mesh sizes;

(4) Evaluate the structure-side heat transfer coefficients and heat transfer areas to be used in the calculations of can wall heat transfer, fuel pin heat transfer and fluid heat and mass transfer; and

(5) Calculate the hydraulic diameter for each mesh cell, based on the structure volume fractions and surface areas per unit volume.

First the flags are defined as to whether the structure-field components are present in each cell:

Pin fuel: NF1 = 1 if $\overline{\rho}_{s1} + \overline{\rho}_{s2} > 0$,

Left crust: NF2 = 1 if $\overline{\rho}_{s3} + \overline{\rho}_{s4} > 0$,

Right crust: NF3 = 1 if $\overline{\rho}_{s5} + \overline{\rho}_{s6} > 0$,

Cladding: NCL = 1 if $\overline{\rho}_{s7} > 0$,

Left can wall: NCANL = 1 if $\overline{\rho}_{s9} > 0$,

Right can wall: NCANR = 1 if $\overline{\rho}_{s11} > 0$, and

Control: NCON = 1 if $\overline{\rho}_{s12} > 0$.

Then the indexes are defined as follows for the surface nodes of three structures that

are in contact with fluid.

$k1$: fuel pin surface (either cladding or pin fuel surface),

$k2$: left can wall surface (either crust fuel, can wall surface or interior), and

$k3$: right can wall surface (either crust fuel, can wall surface or interior).

These indexes are transferred to the heat and mass transfer model, and are used to identify the component with which heat and mass are exchanged with fluid. The control pin is treated similarly to fuel pin, but there is no mass transfer path from solid control.

It is noted that the structure heat-transfer coefficients are generally limited to a certain minimum value, considering the stability of heat-transfer calculations.

4.2. Can-Wall Configuration

4.2.1. Can wall configuration cases

There are three situations, each of which has three cases as to presence and inter-cell coupling of can wall, when the locations of radial cells are considered. As described previously, only a right cell boundary is considered for a normal mesh cell ($2 \le i \le IB-1$). The typical cases of the can wall configuration are shown in Fig. 4-1.

(1) Left cell boundary for the first real cell in a row ($i=1$)

In this case, the single left can wall only contacts locally with fluid in the same mesh cell. Three cases exist as follows:

Case 1 (one can wall node): NCANL = 1 ,

Case 2 (two can wall nodes): NCANL = 1 , and

Case 3 (no can wall): NCANL = 0

In Cases 1 and 2, the crust fuel if present is coupled with the can wall.

(2) Right cell boundary for the last real cell in a row ($i = IB$)

In this situation, the single right can wall in present only contacts locally with fluid in the same mesh cell. Three cases exist as follows:

Case 4 (One structure node): $NCANR = 1$,

Case 5 (Two structure nodes): $NCANR = 1$, and

Case 6 (No can wall structure): $NCANR = 0$.

In Cases 4 and 5, the crust fuel if present is coupled with the can wall.

(3) Right cell boundary of normal real cell ($2 \le i \le IB-1$)

In this situation, two adjacent mesh cells are considered, and up to two can walls can exist, one from the cell and the other from the right-adjacent cell. The treatment applies to all the radial cells except for the rightmost real cell ($i = IB$). Three cases exist as follows:

Case 7 (two can walls): $NCANL(ij+1) + NCANR(ij) = 2$

Case 8 (only one can wall): $NCANL(ij+1) + NCANR(ij) = 1$

Case 9 (no can wall): $NCANL(ij+1) + NCANR(ij) = 0$

In Case 7, the two can walls in two adjacent cells are thermally decoupled each other. There are two sub-cases for each can wall, depending on the thickness and hence the number of nodes. Coupling of the crust fuel if present with can wall is treated similarly to Cases 1, 2, 4 and 5.

In Case 8, the two cells are thermally coupled through a single can wall placed at the in-between mesh cell boundary. The crust fuel can be placed on both the can wall surfaces when it exists. Both thin and thick sub-cases are modeled. A thin can wall is represented by a single interior node, whilst a thick can wall is represented by an interior node and two surface nodes on both sides. In the latter sub-case, a part of the can wall interior mass is taken from this cell and is set over as the surface node to the adjacent cell. This procedure of set-over of the surface node allows us to calculate the inter-cell heat and mass transfer. However, the volume fraction of the set-over can wall surface node is added to the original cell where the interior node exists. This treatment is rather complex but is required to conserve the structure volume fraction and the flow area in the two cells.

No structure configuration is defined in Case 9, in which no can wall exists. Radial fluid flow is allowed only in this case.

4.2.2. Can wall thickness

The selection of can wall configuration cases depends on the can wall thickness. When the wall thickness is calculated, there is some difference between the slab geometry and the cylindrical geometry. For the slab geometry, the thicknesses are calculated by

$$W_{LCW} = \left[\alpha_{S5} + \alpha_{S6} + \alpha_{S7,ij-1} \frac{V_{ij-1}}{V_{ij}} \right] \Big/ a_{LCW} \quad \text{, for the left can wall, and} \tag{4-1}$$

$$W_{RCW} = \left[\alpha_{S7} + \alpha_{S8} + \alpha_{S5,ij+1} \frac{V_{ij+1}}{V_{ij}} \right] \Big/ a_{RCW} \quad \text{, for the right can wall,} \tag{4-2}$$

where V_{ij} a_{LCW} and a_{RCW} are the cell volume, left and right can wall surface areas, respectively, of cell *ij*, and V_{ij+1} is the cell volume of cell *ij+1*.

For the cylindrical geometry, the thicknesses are calculated by

$$W_{LCW} = \sqrt{r_{C0}^2 + \left(r_{C1}^2 - r_{C0}^2\right)\left(\alpha_{S5} + \alpha_{S6} + \alpha_{S7,ij-1} \frac{V_{ij-1}}{V_{ij}} \right)} - r_{C0}, \tag{4-3}$$

for the left can wall, and

$$W_{RCW} = r_{C1} - \sqrt{r_{C0}^2 + \left(r_{C1}^2 - r_{C0}^2\right)\left[1 - \left(\alpha_{S7} + \alpha_{S8} + \alpha_{S5,ij-1} \frac{V_{ij-1}}{V_{ij}} \right) \right]}, \tag{4-4}$$

for the right can wall, where r_{C0} and r_{C1} are radii of the left and right boundary of cell ij, respectively.

The term with the cell volume ratio is required in both cases to conserve can wall mass when the surface node is set over to the adjacent cell where no can wall exists initially. The cylindrical geometry defines the surface areas per unit volume in each time step, whereas the slab geometry applies the input constant values.

The thickness of a can wall surface node is determined from the steel thermal penetration distance, $2\delta_s$, in both cases. The criterion that the can wall is thin is judged by the thickness of the interior node which must be greater than $2\delta_s$. Therefore, in Cases 1, 2, 4, 5, and 7, in which a surface node is placed on one side of the

wall, the can wall is regarded as thin if $W \le 4\delta_s$, and in Case 8, in which the surface nodes are placed on both sides of the wall, the can wall is regarded as thin if $W \le 6\delta_s$.

4.2.3. Can wall configurations for the left boundary of the first real cell

(1) Case 1 (thin can wall)

If the can wall is regarded as thin, namely if $W \le 4\delta_s$, all the can wall mass is represented by the interior node.

(a) The slab geometry

The macroscopic densities and specific internal energies are calculated by

$$\tilde{\overline{\rho}}_{s9}^{n+1} = \overline{\rho}_{s8}^{n} + \overline{\rho}_{s9}^{n}; \quad \tilde{\overline{\rho}}_{s8}^{n+1} = 0 \quad \text{, and} \tag{4-5}$$

$$\tilde{e}_{S6}^{n+1} = \frac{\overline{\rho}_{s8}^{n} e_{S5}^{n} + \overline{\rho}_{s9}^{n} e_{S6}^{n}}{\tilde{\overline{\rho}}_{s9}^{n+1}}; \quad \tilde{e}_{S5}^{n+1} = e_{S,2}^{0} \quad , \tag{4-6}$$

where the superscript n denotes the fluid time step number and tilde variables are the intermediate end-of-time-step values updated by this model. The zero internal energy for steel, $e_{S,2}^{0}$, is the minimum solid specific internal energy defined in EOS.

When the can wall is modeled by the slab geometry, the structure heat-transfer area is set equal to the initial value whether the crust fuel exists or not.

$$a_{LCW} = a_{LCW}^{i}. \tag{4-7}$$

If the crust fuel exists, it contacts with fluid in the cell and the structure-side heat-transfer coefficient is given by

$$h_{S2} = \frac{2\kappa_f a_{LCW}}{\alpha_{S2}^{n}}, \text{ and.} \tag{4-8}$$

$$h_{k2} = \min\left[\frac{(\overline{\rho}_{s3} + \overline{\rho}_{s4}) c_{S2}}{\Delta t a_{LCW}}, h_{S2} \right] \quad , \tag{4-9}$$

When the fuel crust becomes thin, the heat-transfer calculation can be unstable. Thus, the structure-side heat-transfer coefficient is limited such that the heat transferred does not exceed the heat capacity.

If the crust does not exist, fluid is assumed to directly contacts with the can wall and the structure side heat-transfer coefficient is given by

$$h_{S6} = \frac{2\kappa_s a_{LCW}}{\tilde{\alpha}_{S6}^{n+1}}, \text{ and} \tag{4-10}$$

$$h_{k2} = \min\left[\frac{\tilde{\bar{\rho}}_{s9}^{n+1} c_{S6}}{\Delta t a_{LCW}}, h_{S6}\right] . \tag{4-11}$$

The heat-transfer coefficient between the crust and the can wall is given by

$$h_{S2,S6} = \frac{h_{S2} h_{S6}}{h_{S2} + h_{S6}} . \tag{4-12}$$

(b) The cylindrical geometry

When the can wall is represented by the cylindrical geometry, it is necessary to define each radius of node boundaries and of temperature points at first. They are shown in Fig. 4-2.

The radii of the can wall surface and the temperature point are respectively given by

$$r_4 = r_{C0} + W_{LCW} \quad \text{and} \quad r_{t4} = \sqrt{\left(r_{C0}^2 + r_4^2\right)/2}\,, \tag{4-13}$$

where r_{C0} is radius of the left boundary of the cell and $r_{C0} = 0$ in this case.

The macroscopic densities are calculated by

$$\tilde{\bar{\rho}}_{s9}^{n+1} = \frac{1}{v_s}\frac{r_4^2 - r_{C0}^2}{r_{C1}^2 - r_{C0}^2} \quad \text{and} \quad \tilde{\bar{\rho}}_{s8}^{n+1} = 0 \quad , \tag{4-14}$$

where r_{C1} is radius of the right boundary of the cell, and the specific internal energies are defined using Eq. (4-6).

If the crust fuel does not exist, the heat transfer coefficient of the structure side is given by

$$h_{S6} = \frac{\kappa_s}{r_4 \ln\left(r_4 / r_{t4}\right)} \quad \text{, and} \tag{4-15}$$

$$h_{k2} = \min\left[\frac{\tilde{\bar{\rho}}_{s9}^{n+1} c_{S6}}{\Delta t a_{LCW}}, h_{S6}\right]. \tag{4-16}$$

The surface area of the structure which is in contact with fluid is defined by

$$a_{LCW} = \frac{2r_4}{r_{C1}^2 - r_{C0}^2} \quad . \tag{4-17}$$

If the crust fuel exists, the heat transfer coefficient of the structure side is given by

$$h_{S2} = \frac{\kappa_f}{r_6 \ln(r_6 / r_{t6})} \quad \text{and} \tag{4-18}$$

$$h_{k2} = \min\left[\frac{(\overline{\rho}_{s3} + \overline{\rho}_{s4}) c_{S2}}{\Delta t a_{LCW}}, h_{S2} \right], \tag{4-19}$$

where r_6 and r_{t6} are calculated by

$$r_6 = \sqrt{r_{C0}^2 + (r_{C1}^2 - r_{C0}^2)(\alpha_{S2}^n + \tilde{\alpha}_{S5}^{n+1} + \tilde{\alpha}_{S6}^{n+1})}, \text{ and } \quad r_{t6} = \sqrt{(r_4^2 + r_6^2)/2} \, . \tag{4-20}$$

The surface area of the structure which is in contact with fluid is defined by

$$a_{LCW} = \frac{2r_6}{r_{C1}^2 - r_{C0}^2} . \tag{4-21}$$

The heat transfer area and the heat transfer coefficient between the crust and the can wall are respectively given by,

$$a_{S2,S6} = \frac{2r_4}{r_{C1}^2 - r_{C0}^2} \quad , \text{ and} \tag{4-22}$$

$$h_{S2,S6} = \frac{1}{r_4 \left[\kappa_s^{-1} \ln(r_4 / r_{t4}) + \kappa_f^{-1} \ln(r_{t6} / r_4) \right]} \quad . \tag{4-23}$$

(2) Case 2 (thick can wall)

If the can wall is regarded as thick, $W > 4\delta_s$, the surface node thickness is set to be constant ($2\delta_s$).

(a) The slab geometry

The rezoning algorithm for the slab geometry is applied as

$$\tilde{\overline{\rho}}_{s8}^{n+1} = \frac{2\delta_s}{W_{LCW}} \left(\overline{\rho}_{s8}^n + \overline{\rho}_{s9}^n \right) \ , \tag{4-24}$$

$$\tilde{\overline{\rho}}_{s9}^{n+1} = \overline{\rho}_{s8}^n + \overline{\rho}_{s9}^n - \tilde{\overline{\rho}}_{s8}^{n+1} , \tag{4-25}$$

$$\tilde{e}_{S5}^{n+1} = \begin{cases} e_{S5}^{n} & if \quad \tilde{\bar{\rho}}_{s8}^{n+1} < \bar{\rho}_{s8}^{n} \\ \dfrac{\left[\bar{\rho}_{s8}^{n} e_{S5}^{n} + \left(\tilde{\bar{\rho}}_{s8}^{n+1} - \bar{\rho}_{s8}^{n}\right) e_{S6}^{n}\right]}{\tilde{\bar{\rho}}_{s8}^{n+1}} & if \quad \tilde{\bar{\rho}}_{s8}^{n+1} \geq \bar{\rho}_{s8}^{n} \end{cases} , \text{ and} \tag{4-26}$$

$$\tilde{e}_{S6}^{n+1} = \begin{cases} \dfrac{\left[\bar{\rho}_{s9}^{n} e_{S6}^{n} + \left(\tilde{\bar{\rho}}_{s9}^{n+1} - \bar{\rho}_{s9}^{n}\right) e_{S5}^{n}\right]}{\tilde{\bar{\rho}}_{s9}^{n+1}} & if \quad \tilde{\bar{\rho}}_{s9}^{n+1} \geq \bar{\rho}_{s9}^{n} \\ e_{S6}^{n} & if \quad \tilde{\bar{\rho}}_{s9}^{n+1} < \bar{\rho}_{s9}^{n} \end{cases} . \tag{4-27}$$

If the crust fuel exists, the heat-transfer coefficient for the crust is calculated, similarly to Case 1. The heat-transfer coefficients for the two can wall nodes are

$$h_{S5} = \frac{2\kappa_s a_{LCW}}{\tilde{\alpha}_{S5}^{n+1}} \text{ , and } h_{S6} = \frac{2\kappa_s a_{LCW}}{\tilde{\alpha}_{S6}^{n+1}} . \tag{4-28}$$

The structure-structure heat-transfer coefficients are then calculated by

$$h_{S2,S5} = \frac{h_{S2} h_{S5}}{h_{S2} + h_{S5}} \text{ , and } h_{S5,S6} = \frac{h_{S5} h_{S6}}{h_{S5} + h_{S6}} . \tag{4-29}$$

The structure-side heat-transfer coefficient is given by

$$h_{k2} = \min\left[\frac{\left(\bar{\rho}_{s3}^{n} + \bar{\rho}_{s4}^{n}\right) c_{S2}}{\Delta t a_{LCW}}, h_{S2}\right] \text{ , if crust exists, or} \tag{4-30}$$

$$h_{k2} = \min\left[\frac{\tilde{\bar{\rho}}_{s8}^{n+1} c_{S5}}{\Delta t a_{LCW}}, h_{S5}\right] \text{ , if crust does not exist.} \tag{4-31}$$

(b) The cylindrical geometry

Each radius of the node boundaries and of temperature points is shown in Fig. 4-2. The rezoning algorithm for the cylindrical geometry is applied as

$$r_5 = \sqrt{r_{C0}^2 + \left(r_{C1}^2 - r_{C0}^2\right)\left(\alpha_{S5}^{n} + \alpha_{S6}^{n}\right)} \quad , \quad r_4 = r_5 - 2\delta_s \quad , \tag{4-32}$$

$$\tilde{\bar{\rho}}_{s8}^{n+1} = \frac{1}{v_s} \frac{r_5^2 - r_4^2}{r_{C1}^2 - r_{C0}^2} \text{ and } \tilde{\bar{\rho}}_{s9}^{n+1} = \frac{1}{v_s} \frac{r_4^2 - r_{C0}^2}{r_{C1}^2 - r_{C0}^2} \quad , \tag{4-33}$$

Their specific internal energies are defined using Eqs. (4-26) and (4-27).

If the crust fuel does not exist, the surface area of the structure and the heat transfer coefficient of the structure-side are respectively given by

$$a_{LCW} = \frac{2r_5}{r_{C1}^2 - r_{C0}^2}, \tag{4-34}$$

$$h_{S5} = \frac{\kappa_s}{r_5 \ln(r_5/r_{t5})} \text{ , where } r_{t5} = \sqrt{(r_4^2 + r_5^2)/2} \text{ and} \tag{4-35}$$

$$h_{k2} = \min\left[\frac{\tilde{\tilde{\rho}}_{s8}^{n+1} c_{S5}}{\Delta t a_{LCW}}, h_{S5}\right]. \tag{4-36}$$

If the crust fuel exists, the heat-transfer coefficient for the crust and the can wall surface area are calculated, similarly to Case 1.

The heat transfer coefficient of the interior node, the structure-structure heat transfer area and the intra-structure heat transfer coefficient are given by

$$h_{S6} = \frac{\kappa_s}{r_4 \ln(r_4/r_{t4})} \text{ , where } r_{t4} = \sqrt{(r_4^2 + r_{C0}^2)/2}, \tag{4-37}$$

$$a_{S5,S6} = \frac{2r_4}{r_{C1}^2 - r_{C0}^2} \text{ , and} \tag{4-38}$$

$$h_{S5,S6} = \frac{1}{r_4\left[\kappa_s^{-1} \ln(r_{t5}/r_4) + \kappa_s^{-1} \ln(r_4/r_{t4})\right]} \text{ .} \tag{4-39}$$

If the crust exists, the followings are defined:

$$a_{S2,S5} = \frac{2r_5}{r_{C1}^2 - r_{C0}^2}, \text{ and } h_{S2,S5} = \frac{1}{r_5\left[\kappa_s^{-1} \ln(r_5/r_{t5}) + \kappa_f^{-1} \ln(r_{t6}/r_5)\right]} \text{ ,} \tag{4-40}$$

where,

$$r_6 = \sqrt{r_{C0}^2 + (r_{C1}^2 - r_{C0}^2)(\alpha_{S2}^n + \alpha_{S5}^n + \alpha_{S6}^n)} \text{ and } r_{t6} = \sqrt{(r_5^2 + r_6^2)/2} \text{ .} \tag{4-41}$$

4.2.4. Can wall configurations for the right boundary of the normal real cell

(1) Case 7

Two can walls are separate each other and the two adjacent cells are thermally decoupled. The can walls are simply treated independently, and the same procedure is applied to each of the can wall as one used in Cases 1, 2, 4 and 5.

(2) Sub-cases for Case 8

In this case, there are four sub-cases depending on whether the can wall is thin nor thick and whether the crust exists or not. These sub-cases are defined as

Case 8a represents a thin can wall and $NF2 + NF3 = 0$,

Case 8b represents a thin can wall and $NF2 + NF3 > 0$,

Case 8c represents a thick can wall and $NF2 + NF3 = 0$, and

Case 8d represents a thick can wall and $NF2 + NF3 > 0$.

(3) Case 8a (thin can wall without crust)

The objective is to combine any existing surface node into the main interior node and then to have this interior node contact with fluid on both sides of the cell boundary.

(a) The slab geometry

If there is a left can wall in the right adjacent cell ($NCANL(IJ+1) > 0$), the algorithm used for the slab geometry in combining the three can wall nodes is written as

$$\tilde{\bar{\rho}}_{s9}^{n+1}(ij+1) = \bar{\rho}_{s8}^{n}(ij+1) + \bar{\rho}_{s9}^{n}(ij+1) + \bar{\rho}_{s10}^{n}(ij)\frac{V_{ij}}{V_{ij+1}}, \text{ and} \tag{4-42}$$

$$\tilde{e}_{S6}^{n+1}(ij+1) = \frac{\left[\bar{\rho}_{s8}^{n}(ij+1)e_{S5}^{n}(ij+1) + \bar{\rho}_{s9}^{n}(ij+1)e_{S6}^{n}(ij+1) + \bar{\rho}_{s10}^{n}(ij)\frac{V_{ij}}{V_{ij+1}}e_{S7}^{n}(ij)\right]}{\tilde{\bar{\rho}}_{s9}^{n+1}(ij+1)}. \tag{4-43}$$

If there is a right can wall in the cell ($NCANR(IJ) > 0$), the combination algorithm for the slab geometry is

$$\tilde{\bar{\rho}}_{s11}^{n+1}(ij) = \bar{\rho}_{s8}^{n}(ij+1)\frac{V_{ij+1}}{V_{ij}} + \bar{\rho}_{s10}^{n}(ij) + \bar{\rho}_{s11}^{n}(ij), \text{ and} \tag{4-44}$$

$$\tilde{e}_{S8}^{n+1}(ij) = \frac{\left[\bar{\rho}_{s8}^{n}(ij+1)\frac{V_{ij+1}}{V_{ij}}e_{S5}^{n}(ij+1) + \bar{\rho}_{s10}^{n}(ij)e_{S7}^{n}(ij) + \bar{\rho}_{s11}^{n}(ij)e_{S8}^{n}(ij)\right]}{\tilde{\bar{\rho}}_{s11}^{n+1}(ij)}. \tag{4-45}$$

In these combinations the macroscopic densities of surface nodes are set to zero.

$$\tilde{\bar{\rho}}_{s8}^{n+1}(ij+1) = 0, \quad \tilde{\bar{\rho}}_{s10}^{n+1}(ij) = 0, \quad \tilde{e}_{S5}^{n+1}(ij+1) = e_{S,2}^{0}, \text{ and } \quad \tilde{e}_{S7}^{n+1}(ij) = e_{S,2}^{0}. \tag{4-46}$$

The combining procedure requires the transfer, crossing over the mesh cell boundary,

of macroscopic density and specific internal energy of the surface node of the adjacent cell. To conserve the mass in this combination, the macroscopic density transferred is multiplied by the cell volume ratio. Similarly, when the can wall surface area is transferred, this is also multiplied by the volume ratio.

If there is a left can wall in the right adjacent cell ($NCANL(IJ+1) > 0$), the surface area, the heat-transfer coefficient for the existing can wall and the structure-side heat-transfer coefficients are given by

$$a_{LCW}(ij+1) = a^{i}_{LCW}(ij+1), \tag{4-47}$$

$$a_{RCW}(ij) = a^{i}_{LCW}(ij+1)\frac{V_{ij+1}}{V_{ij}}, \tag{4-48}$$

$$h_{S6}(ij+1) = \frac{2\kappa_s a_{LCW}(ij+1)}{\tilde{\alpha}^{n+1}_{S6}(ij+1)}, \text{ and} \tag{4-49}$$

$$h_{k3} = h_{k2}(ij+1) = \min\left[\frac{\tilde{\tilde{\rho}}^{n+1}_{s9}(ij+1)c_{S6}(ij+1)}{\Delta t a_{LCW}(ij+1)}, h_{S6}(\mathrm{ij}+1)\right]. \tag{4-50}$$

If there is a right can wall in the cell ($NCANR(IJ) > 0$), they are

$$a_{RCW}(ij) = a^{i}_{RCW}(ij), \tag{4-51}$$

$$a_{LCW}(ij+1) = a^{i}_{RCW}(ij)\frac{V_{ij}}{V_{ij+1}}, \tag{4-52}$$

$$h_{S8}(ij) = \frac{2\kappa_s a_{RCW}(ij)}{\tilde{\alpha}^{n+1}_{S8}(ij)}, \text{ and} \tag{4-53}$$

$$h_{k3} = h_{k2}(ij+1) = \min\left[\frac{\tilde{\tilde{\rho}}^{n+1}_{s11}(ij)c_{S8}(ij)}{\Delta t a_{RCW}(ij)}, h_{S8}(\mathrm{ij})\right]. \tag{4-54}$$

(b) The cylindrical geometry

Each radius of the node boundaries and of temperature points is shown in Fig. 4-2. When the cylindrical geometry is used, the algorithm adopted in combining the three can wall nodes is obtained by replacing the Eqs. (4-42) and (4-44) with

$$\tilde{\tilde{\rho}}^{n+1}_{s9}(ij+1) = \frac{1}{v_s}\frac{r_4^2 - r_{C1}^2}{r_{C2}^2 - r_{C1}^2}, \text{ if } NCANL(IJ+1) > 0, \text{ and} \tag{4-55}$$

$$\tilde{\tilde{\rho}}_{s11}^{n+1}(ij) = \frac{1}{v_s}\frac{r_{C1}^2 - r_3^2}{r_{C1}^2 - r_{C0}^2}, \text{ if } NCANR(IJ) > 0 , \tag{4-56}$$

where r_{C0} and r_{C1} are radii of the left and right boundary of cell ij respectively, r_{C2} is the right boundary of cell ij+1, and r_3 and r_4 are given by

$$r_3 = r_{C1} - W_{RCW} \quad \text{and} \quad r_4 = r_{C1} + W_{LCW} \quad . \tag{4-57}$$

If there is a left can wall in the right adjacent cell ($NCANL(IJ+1) > 0$), the surface area, the heat-transfer coefficient for the existing can wall and the structure-side heat-transfer coefficients are given by

$$a_{LCW}(ij+1) = \frac{2r_4}{r_{C2}^2 - r_{C1}^2}, \tag{4-58}$$

$$a_{RCW}(ij) = \frac{2r_{C1}}{r_{C1}^2 - r_{C0}^2}, \tag{4-59}$$

$$h_{S6}(ij+1) = \frac{\kappa_s}{r_4 \ln(r_4/r_{t4})}, \text{ where } r_{t4} = \sqrt{(r_{C1}^2 + r_4^2)/2} \text{ , and} \tag{4-60}$$

$$h_{k3}(ij) = h_{k2}(ij+1) = \min\left[\frac{\tilde{\tilde{\rho}}_{s9}^{n+1}(ij+1)c_{S6}(ij+1)}{\Delta t a_{LCW}(ij+1)}, h_{S6}(ij+1)\right]. \tag{4-61}$$

If there is a right can wall in the cell ($NCANR(IJ) > 0$), they are

$$a_{RCW}(ij) = \frac{2r_3}{r_{C1}^2 - r_{C0}^2}, \tag{4-62}$$

$$a_{LCW}(ij+1) = \frac{2r_{C1}}{r_{C2}^2 - r_{C1}^2}, \tag{4-63}$$

$$h_{S8}(ij) = \frac{\kappa_s}{r_3 \ln(r_{t3}/r_3)}, \text{ where } r_{t3} = \sqrt{(r_3^2 + r_{C1}^2)/2} \text{ , and} \tag{4-64}$$

$$h_{k2}(ij+1) = h_{k3}(ij) = \min\left[\frac{\tilde{\tilde{\rho}}_{s11}^{n+1}(ij)c_{S8}(ij)}{\Delta t a_{RCW}(ij)}, h_{S8}(ij+1)\right]. \tag{4-65}$$

(4) Case 8b (thin can wall with crust)

(a) The slab geometry

First, the can wall surface nodes need to be combined using Eqs. (4-42) - (4-46) as in

Case 8a. Second, the heat-transfer coefficients for existing can wall are still given by Eq. (4-49). Third, the heat-transfer coefficients for the crusts are

$$h_{S2}(ij+1)=\frac{2\kappa_f a_{LCW}(ij+1)}{\alpha^n_{S2}(ij+1)}, \text{ and } \; h_{S3}(ij)=\frac{2\kappa_f a_{RCW}(ij)}{\alpha^n_{S3}(ij)} \quad . \tag{4-66}$$

In this case, the structure outer surface is always the crust, so that the structure-side heat-transfer coefficients are determined from

$$h_{k2}(ij+1)=\min\left[\frac{\left[\overline{\rho}^n_{s3}(ij+1)+\overline{\rho}^n_{s4}(ij+1)\right]c_{S2}(ij+1)}{\Delta t a_{LCW}(ij+1)}, h_{S2}(ij+1)\right], \text{ and} \tag{4-67}$$

$$h_{k3}(ij)=\min\left[\frac{\left[\overline{\rho}^n_{s5}(ij)+\overline{\rho}^n_{s6}(ij)\right]c_{S3}(ij)}{\Delta t a_{RCW}(ij)}, h_{S3}(ij)\right] \quad . \tag{4-68}$$

If there is a right can wall in the cell ($NCANR(IJ) > 0$), there are two definitions for heat-transfer coefficient between the crust and the can wall whether a crust exists in the same cell ($NF3(IJ) > 0$) or in the right adjacent cell ($NF2(IJ+1) > 0$). In the former case, it is

$$h_{S3,S8}(ij)=\frac{h_{S3}(ij)h_{S8}(ij)}{h_{S3}(ij)+h_{S8}(ij)} \quad , \tag{4-69}$$

and in the latter case, an overall cross-cell product of interfacial area and heat-transfer coefficient is

$$(ha)_{S2(ij+1),S8(ij)}=\frac{a_{RCW}(ij)h_{S8}(ij)h_{S2}(ij+1)}{h_{S8}(ij)+h_{S2}(ij+1)} \quad . \tag{4-70}$$

If there is a left can wall in the right adjacent cell ($NCANL(IJ+1) > 0$), the same equations are available if subscripts of right components replace those of left components.

(b) The cylindrical geometry

Each radius of the node boundaries and of temperature points is shown in Fig. 4-2. The can wall surface nodes need to be combined as in Case 8a. If there is a right can wall in the cell ($NCANR(IJ) > 0$), the heat-transfer coefficients for the crusts are

$$h_{S2}(ij+1)=\frac{\kappa_f}{r_6\ln(r_6/r_{t6})} \quad \text{and} \quad h_{S3}(ij)=\frac{\kappa_f}{r_1\ln(r_{t1}/r_1)} \quad , \tag{4-71}$$

where each radius is given by

$$r_6=\sqrt{r_{C1}^2+(r_{C2}^2-r_{C1}^2)\alpha_{S2}^n(ij+1)}, \quad r_{t6}=\sqrt{(r_{C1}^2+r_6^2)/2} \quad ,$$

$$r_1=\sqrt{r_{C0}^2+(r_{C1}^2-r_{C0}^2)\left[1-(\alpha_{S3}^n(ij)+\alpha_{S8}^n(ij))\right]}, \text{ and } \quad r_{t1}=\sqrt{(r_1^2+r_{C1}^2)/2}\,. \tag{4-72}$$

Since the crust fuel is in contact with fluid, the structure surface areas are given by

$$a_{RCW}(ij)=\frac{2r_1}{r_{C1}^2-r_{C0}^2} \quad \text{and} \quad a_{LCW}(ij+1)=\frac{2r_6}{r_{C2}^2-r_{C1}^2}\,. \tag{4-73}$$

The structure-side heat-transfer coefficients are determined from Eqs. (4-67) and (4-68).

The heat transfer coefficient and the heat transfer area between the crust and the can wall in the same cell are given by

$$h_{S3,S8}(ij)=\frac{1}{r_3\left[\kappa_f^{-1}\ln(r_3/r_{t1})+\kappa_s^{-1}\ln(r_{t3}/r_3)\right]} \quad \text{, where} \quad r_{t3}=\sqrt{(r_3^2+r_{C1}^2)/2} \text{ , and} \tag{4-74}$$

$$a_{S3,S8}(ij)=\frac{2r_3}{r_{C1}^2-r_{C0}^2}\,. \tag{4-75}$$

An overall cross-cell product of interfacial area and heat-transfer coefficient are given by

$$a_{S2(ij+1),S8(ij)}=2r_{C1}/(r_{C1}^2-r_{C0}^2) \quad \text{, and} \tag{4-76}$$

$$(ha)_{S2(ij+1),S8(ij)}=\frac{a_{S2(ij+1),S8(ij)}}{r_{C1}\left[\kappa_s^{-1}\ln(r_{C1}/r_{t3})+\kappa_f^{-1}\ln(r_{t6}/r_{C1})\right]} \quad . \tag{4-77}$$

The same equations are available for a left can wall in the right adjacent cell (NCANL(IJ+1) > 0) by replacing subscripts of right components with those of left components.

(5) Case 8c (thick can wall without crust)

The objective is to maintain a configuration where the existing can wall interior

node has two surface nodes, one of which is in an adjacent cell. First, if the surface nodes either do not exist or are too small, rezoning is required.

(a) The slab geometry

If there is a left can wall in an adjacent cell ($NCANL(IJ+1) > 1$), the rezoning algorithm is

$$\tilde{\bar{\rho}}_{s8}^{n+1}(ij+1)=\frac{2\delta_s}{W_{LCW}}\left[\bar{\rho}_{s8}^{n}(ij+1)+\bar{\rho}_{s9}^{n}(ij+1)+\bar{\rho}_{s10}^{n}(ij)\frac{V_{ij}}{V_{ij+1}}\right], \tag{4-78}$$

$$\tilde{\bar{\rho}}_{s10}^{n+1}(ij)=\frac{2\delta_s}{W_{LCW}}\left[\bar{\rho}_{s8}^{n}(ij+1)\frac{V_{ij+1}}{V_{ij}}+\bar{\rho}_{s9}^{n}(ij+1)\frac{V_{ij+1}}{V_{ij}}+\bar{\rho}_{s10}^{n}(ij)\right], \tag{4-79}$$

$$\tilde{\bar{\rho}}_{s9}^{n+1}(ij+1)=\bar{\rho}_{s8}^{n}(ij+1)+\bar{\rho}_{s9}^{n}(ij+1)+\bar{\rho}_{s10}^{n}(ij)\frac{V_{ij}}{V_{ij+1}}-\tilde{\bar{\rho}}_{s8}^{n+1}(ij+1)-\bar{\rho}_{s10}^{n}(ij)\frac{V_{ij}}{V_{ij+1}}, \tag{4-80}$$

$$\tilde{e}_{S5}^{n+1}(ij+1)=$$

$$\begin{cases} e_{S5}^{n}(ij+1) & \text{if } \tilde{\bar{\rho}}_{s8}^{n+1}(ij+1)<\bar{\rho}_{s8}^{n}(ij+1) \\ \dfrac{\bar{\rho}_{s8}^{n}(ij+1)e_{S5}^{n}(ij+1)+\left[\tilde{\bar{\rho}}_{s8}^{n+1}(ij+1)-\bar{\rho}_{s8}^{n}(ij+1)\right]e_{S6}^{n}(ij+1)}{\tilde{\bar{\rho}}_{s8}^{n+1}(ij)} & \\ & \text{if } \tilde{\bar{\rho}}_{s8}^{n+1}(ij+1)\geq\bar{\rho}_{s8}^{n}(ij+1) \end{cases} \tag{4-81}$$

$$\tilde{e}_{S7}^{n+1}(ij)=\begin{cases} e_{S7}^{n}(ij) & \text{if } \tilde{\bar{\rho}}_{s10}^{n+1}(ij)<\bar{\rho}_{s10}^{n}(ij) \\ \dfrac{\bar{\rho}_{s10}^{n}(ij)e_{S7}^{n}(ij)+\left[\tilde{\bar{\rho}}_{s10}^{n+1}(ij)-\bar{\rho}_{s10}^{n}(ij)\right]e_{S6}^{n}(ij+1)}{\tilde{\bar{\rho}}_{s10}^{n+1}(ij)} & \text{if } \tilde{\bar{\rho}}_{s10}^{n+1}(ij)\geq\bar{\rho}_{s10}^{n}(ij) \end{cases}, \quad \text{and} \tag{4-82}$$

$$\tilde{e}_{S6}^{n+1}(ij+1)=$$

$$\begin{cases} e_{S6}^{n}(ij+1) & \text{if } \tilde{\bar{\rho}}_{s8}^{n+1}(ij+1)\geq\bar{\rho}_{s8}^{n}(ij+1) \text{ and } \tilde{\bar{\rho}}_{s10}^{n+1}(ij)\geq\bar{\rho}_{s10}^{n}(ij) \\ \dfrac{\bar{\rho}_{s9}^{n}(ij+1)e_{S6}^{n}(ij+1)-\left[\tilde{\bar{\rho}}_{s8}^{n+1}(ij+1)-\bar{\rho}_{s8}^{n}(ij+1)\right]e_{S6}^{n}(ij+1)-\left[\tilde{\bar{\rho}}_{s10}^{n+1}(ij)-\bar{\rho}_{s10}^{n}(ij)\right]e_{S7}^{n}(ij)}{\tilde{\bar{\rho}}_{s9}^{n+1}(ij+1)} & \\ & \text{if } \tilde{\bar{\rho}}_{s8}^{n+1}(ij+1)\geq\bar{\rho}_{s8}^{n}(ij+1) \text{ and } \tilde{\bar{\rho}}_{s10}^{n+1}(ij)<\bar{\rho}_{s10}^{n}(ij) \\ \dfrac{\bar{\rho}_{s9}^{n}(ij+1)e_{S6}^{n}(ij+1)-\left[\tilde{\bar{\rho}}_{s8}^{n+1}(ij+1)-\bar{\rho}_{s8}^{n}(ij+1)\right]e_{S5}^{n}(ij+1)-\left[\tilde{\bar{\rho}}_{s10}^{n+1}(ij)-\bar{\rho}_{s10}^{n}(ij)\right]e_{S6}^{n}(ij+1)}{\tilde{\bar{\rho}}_{s9}^{n+1}(ij+1)} & \\ & \text{if } \tilde{\bar{\rho}}_{s8}^{n+1}(ij+1)<\bar{\rho}_{s8}^{n}(ij+1) \text{ and } \tilde{\bar{\rho}}_{s10}^{n+1}(ij)\geq\bar{\rho}_{s10}^{n}(ij) \\ \dfrac{\bar{\rho}_{s9}^{n}(ij+1)e_{S6}^{n}(ij+1)-\left[\tilde{\bar{\rho}}_{s8}^{n+1}(ij+1)-\bar{\rho}_{s8}^{n}(ij+1)\right]e_{S5}^{n}(ij+1)-\left[\tilde{\bar{\rho}}_{s10}^{n+1}(ij)-\bar{\rho}_{s10}^{n}(ij)\right]e_{S7}^{n}(ij)}{\tilde{\bar{\rho}}_{s9}^{n+1}(ij+1)} & \\ & \text{if } \tilde{\bar{\rho}}_{s8}^{n+1}(ij+1)<\bar{\rho}_{s8}^{n}(ij+1) \text{ and } \tilde{\bar{\rho}}_{s10}^{n+1}(ij)<\bar{\rho}_{s10}^{n}(ij) \end{cases} .$$

(4-83)

Because one of surface nodes is placed in the adjacent cell, the surface areas are given by

$$a_{LCW}(ij+1) = a^{i}_{LCW}(ij+1), \text{ for } S5, \text{ and} \tag{4-84}$$

$$a_{RCW}(ij) = a^{i}_{LCW}(ij+1)\frac{V_{ij+1}}{V_{ij}}, \text{ for } S7. \tag{4-85}$$

The heat-transfer coefficients for the two surface nodes are

$$h_{S5}(ij+1) = \frac{2\kappa_s a_{LCW}(ij+1)}{\tilde{\alpha}^{n+1}_{S5}(ij+1)}, \text{ and } h_{S7}(ij) = \frac{2\kappa_s a_{RCW}(ij)}{\tilde{\alpha}^{n+1}_{S7}(ij)} \quad . \tag{4-86}$$

The interior node heat-transfer coefficient is

$$h_{S6}(ij+1) = \frac{2\kappa_s a_{LCW}(ij+1)}{\tilde{\alpha}^{n+1}_{S6}(ij+1)} \quad . \tag{4-87}$$

Since fluid is in contact with the surface nodes on both the sides, structure-side heat-transfer coefficients are

$$h_{k2}(ij+1) = \min\left[\frac{\tilde{\bar{\rho}}^{n+1}_{s8}(ij+1)c_{S5}(ij+1)}{\Delta t a_{LCW}(ij+1)}, h_{S5}(ij+1)\right] \text{ , and} \tag{4-88}$$

$$h_{k3}(ij) = \min\left[\frac{\tilde{\bar{\rho}}^{n+1}_{s10}(ij)c_{S7}(ij)}{\Delta t a_{RCW}(ij)}, h_{S7}(ij)\right] \quad . \tag{4-89}$$

The structure-structure heat-transfer coefficient can be directly given by

$$h_{S5,S6}(ij+1) = \frac{h_{S5}(ij+1)h_{S6}(ij+1)}{h_{S5}(ij+1)+h_{S6}(ij+1)}, \tag{4-90}$$

and an overall cross-cell product of interfacial areas and heat-transfer coefficient is

$$(ha)_{S7(ij),S6(ij+1)} = \frac{a_{LCW}(ij+1)h_{S6}(ij+1)h_{S7}(ij)}{h_{S6}(ij+1)+h_{S7}(ij)} \quad . \tag{4-91}$$

If there is a right can wall in the cell ($NCANR(IJ) > 0$), the same rezoning algorithm and equations for surface areas and heat-transfer coefficients are available.

(b) The cylindrical geometry

As shown in Fig. 4-2, if there is a left can wall in an adjacent cell (*NCANL*(*IJ*+1) > 1) and the cylindrical geometry is used the rezoning algorithm of Eqs. (4-78) - (4-80) is replaced with

$$\tilde{\bar{\rho}}_{s8}^{n+1}(ij+1)=\frac{1}{v_s}\frac{r_5^2-r_4^2}{r_{C2}^2-r_{C1}^2} \quad , \tag{4-92}$$

$$\tilde{\bar{\rho}}_{s10}^{n+1}(ij)=\frac{1}{v_s}\frac{r_2^2-r_{C1}^2}{r_{C2}^2-r_{C1}^2}\frac{V_{ij+1}}{V_{ij}} \quad \text{, and} \tag{4-93}$$

$$\tilde{\bar{\rho}}_{s9}^{n+1}(ij+1)=\frac{1}{v_s}\frac{r_4^2-r_2^2}{r_{C2}^2-r_{C1}^2} \quad , \tag{4-94}$$

where r_{c1} and r_{c2} are radii of the left and right boundary of cell ij+1 respectively, and r_5, r_4 and r_2 are given by

$$r_5=r_{C1}+W_{LCW}\text{,}\quad r_4=r_5-2\delta_s \text{ and } r_2=r_{C0}+2\delta_s \text{ .} \tag{4-95}$$

The surface areas of the can wall are given by

$$a_{LCW}(ij+1)=\frac{2r_5}{r_{C2}^2-r_{C1}^2} \text{ for S5, and} \tag{4-96}$$

$$a_{RCW}(ij)=\frac{2r_{C1}}{r_{C1}^2-r_{C0}^2} \text{ for S7.} \tag{4-97}$$

The heat transfer coefficients for the two surface nodes are

$$h_{S5}(ij+1)=\frac{\kappa_s}{r_5\ln(r_5/r_{t5})} \text{ , and } h_{S7}(ij)=\frac{\kappa_s}{r_{C1}\ln(r_{C1}/r_{t2})} \text{ ,} \tag{4-98}$$

where r_{t5} and r_{t2} are given by

$$r_{t5}=\sqrt{(r_5^2+r_4^2)/2} \text{ and } r_{t2}=\sqrt{(r_{C1}^2+r_2^2)/2} \text{ .} \tag{4-99}$$

The structure side heat-transfer coefficients are also defined using Eqs. (4-88) and (4-89).

The structure-structure heat-transfer coefficient and heat transfer area are given by

$$h_{S5,S6}(ij+1)=\frac{\kappa_s}{r_4[\ln(r_4/r_{t4})+\ln(r_{t5}/r_4)]} \quad \text{, where} \quad r_{t4}=\sqrt{(r_4^2+r_2^2)/2} \quad \text{, and,} \tag{4-100}$$

$$a_{S7(ij),S6(ij+1)}(ij+1)=\frac{2r_2}{r_{C2}^2-r_{C1}^2} \quad . \tag{4-101}$$

An overall cross-cell product of interfacial area and heat-transfer coefficient are given by

$$a_{S5(ij+1),S6(ij+1)}(ij+1)=\frac{2r_4}{r_{C2}^2-r_{C1}^2} \tag{4-102}$$

$$(ha)_{S7(ij),S6(ij+1)}=\frac{a_{S7(ij),S6(ij+1)}}{r_2[\kappa_S^{-1}\ln(r_2/r_{t2})+\kappa_S^{-1}\ln(r_{t4}/r_2)]}, \tag{4-103}$$

The same rezoning algorithm and equations for surface areas and heat-transfer coefficients are available for a right can wall in the cell ($NCANR(IJ) > 0$), by replacing subscripts of left components with those of right components.

(6) Case 8d (thick can wall with crust)

(a) The slab geometry

First, any can wall rezoning occurs as in Eqs. (4-78) - (4-83). Second, heat-transfer coefficients for the can walls are given as Eqs. (4-86) and (4-87). Third, the surface areas to fluid are the same as Case 8c. Forth, heat-transfer coefficients for the crusts are given by

$$h_{S2}(ij+1)=\frac{2\kappa_f a_{LCW}(ij+1)}{\alpha_{S2}^n(ij+1)} \quad \text{, and} \quad h_{S3}(ij)=\frac{2\kappa_f a_{RCW}(ij)}{\alpha_{S3}^n(ij)}. \tag{4-104}$$

It is necessary for this case to add the structure-to-structure heat-transfer coefficients as follows.

$$h_{S2,S5}(ij+1)=\frac{h_{S2}(ij+1)h_{S5}(ij+1)}{h_{S2}(ij+1)+h_{S5}(ij+1)}, \text{ and } \quad h_{S3,S7}(ij)=\frac{h_{S3}(ij)h_{S7}(ij)}{h_{S3}(ij)+h_{S7}(ij)} \quad . \tag{4-105}$$

As mentioned in Case 8b, fluid is in contact with crust; and hence if there is a left crust in the right adjacent cell ($NF2(ij+1) > 1$), the structure-side heat-transfer coefficient is

$$h_{k2}(ij+1)=\min\left[\frac{\left[\overline{\rho}_{s3}^{n+1}(ij+1)+\overline{\rho}_{s4}^{n+1}(ij+1)\right]c_{S2}(ij+1)}{\Delta ta_{LCW}(ij+1)},h_{S2}(ij+1)\right], \tag{4-106}$$

and, if there is a right crust in the cell ($NF3(ij) > 1$), the structure-side heat-transfer coefficient is

$$h_{k3}(ij)=\min\left[\frac{\left[\overline{\rho}_{s5}^{n+1}(ij)+\overline{\rho}_{s6}^{n+1}(ij)\right]c_{S3}(ij)}{\Delta ta_{RCW}(ij)},h_{S3}(ij)\right]. \tag{4-107}$$

(b) The cylindrical geometry

The wall configuration is shown in Fig. 4-2. Any can wall rezoning occurs as in Eqs. (4-92) - (4-94) and (4-81) - (4-83). The heat transfer coefficients for the fuel crusts are given by

$$h_{S2}(ij+1)=\frac{\kappa_f}{r_6\ln(r_6/r_{t6})} \text{ and } h_{S3}(ij)=\frac{\kappa_f}{r_1\ln(r_{t1}/r_1)}, \tag{4-108}$$

where each radius is given by

$$r_6=\sqrt{r_{C1}^2+\left(r_{C2}^2-r_{C1}^2\right)\left[\alpha_{S2}^n(ij+1)+\tilde{\alpha}_{S5}^{n+1}(ij+1)+\tilde{\alpha}_{S6}^{n+1}(ij+1)\right]},\ r_5=r_{C1}+W_{LCW}$$

$$r_{t6}=\sqrt{\left(r_5^2+r_6^2\right)/2}\ ,r_1=\sqrt{r_{C0}^2+\left(r_{C1}^2-r_{C0}^2\right)\left[1-\alpha_{S3}^n(ij)\right]}, \text{ and } r_{t1}=\sqrt{\left(r_1^2+r_{C1}^2\right)/2}\ . \tag{4-109}$$

Since the crusts are in contact with the fluid in this case, the structure side heat-transfer coefficients are defined using Eqs. (4-106) and (4-107).

The surface areas to contact with the fluid are given by

$$a_{LCW}(ij+1)=\frac{2r_6}{r_{C2}^2-r_{C1}^2} \text{ and } a_{RCW}(ij)=\frac{2r_1}{r_{C1}^2-r_{C0}^2}\ . \tag{4-110}$$

It is necessary for this case to define the structure-structure heat transfer coefficients and the crust-wall heat-transfer areas as follows.

$$h_{S2,S5}(ij+1)=\frac{1}{r_5\left[\kappa_f^{-1}\ln(r_{t6}/r_5)+\kappa_s^{-1}\ln(r_5/r_{t5})\right]}\ , \tag{4-111}$$

$$h_{S3,S7}(ij)=\frac{1}{r_{C1}\left[\kappa_f^{-1}\ln(r_{C1}/r_{t1})+\kappa_s^{-1}\ln(r_{t2}/r_{C1})\right]}\ , \tag{4-112}$$

$$a_{S2,S5}(ij+1) = 2r_5 / \left(r_{C2}^2 - r_{C1}^2\right) \ , \tag{4-113}$$

$$a_{S3(ij),S7(ij)}(ij+1) = \frac{2r_{C1}}{r_{C2}^2 - r_{C1}^2} \ , \tag{4-114}$$

where each radius is given by

$$r_{t5} = \sqrt{\left(r_4^2 + r_5^2\right)/2} \ , \ r_{t2} = \sqrt{\left(r_2^2 + r_{C1}^2\right)/2} \ , \ r_4 = r_5 - 2\delta_s \ \text{and} \ r_2 = r_{C1} + 2\delta_s \ . \tag{4-115}$$

4.3. Fuel Pin Configuration

Three cases apparently exist if we consider the fuel pin structure configurations. Since the pin fuel interior is calculated outside the fluid dynamics, only the pellet surface node is treated.

Case 1: Both pin fuel/control and cladding exist. $NF1 + NCON = 1$ and $NCL = 1$

Case 2: Only pin fuel/control exists. $NF1 + NCON = 1$ and $NCL = 0$

Case 3: Only cladding exists. $NF1 + NCON = 0$ and $NCL = 1$

Case 3 has two sub-cases depending on existence of a non-flow volume inside the pin, given by input data. Case 3a is the case where the non-flow volume exists and a hollow cladding is considered, such as in a fission gas plenum region. Case 3b is where the non-flow volume does not exist and a solid column cladding is considered such as in a reflector region.

First, the total fuel pin volume fraction is given by

$$\alpha_{pin} = \alpha_{\text{int}} + \left[\overline{\rho}_{s1} + \overline{\rho}_{s2}\right] v_{S1} + \overline{\rho}_{s7} v_{S4} + \overline{\rho}_{s12} v_{S9} + \alpha_{nf,PIN} \ , \tag{4-116}$$

which reflects the change in fuel-pin geometry due to thermal expansion or heat and mass exchange with fluid. The macroscopic density of pin fuel interior represents the energy component including both fertile and fissile pin fuel.

(1) Case 1 (both pin fuel/control and cladding)

Since the pin fuel or control is treated as a cylindrical structure, the radii of three temperature nodes need to be calculated first as shown in Fig. 4-3. Then, geometrical changes are considered, which includes thermal expansion of pin fuel/control and steel freezing and ablation of the cladding surface. The former effect is absorbed into the gap

between the pin fuel/control and the cladding if it is present, otherwise the cladding expands. The latter is represented by increase or decrease of the cladding outer radius. The radii of temperature nodes are set to each structure volumetric centroid. Therefore, they are

$$r_{p6} = r_{PIN} = r_{PIN}^{i}\sqrt{\frac{\alpha_{PIN}}{\alpha_{PIN}^{i}}}\,,\quad r_{p4} = r_{PIN}\sqrt{\frac{a_{\mathrm{int}} + \alpha_{S1} + \alpha_{nf,PIN}}{a_{PIN}}}\,,\quad r_{p3} = r_{PIN}\sqrt{\frac{a_{\mathrm{int}} + \alpha_{S1}}{a_{PIN}}}\,,$$

$$r_{p1} = r_{p3} - 2\delta_f\,,\quad r_{p5} = \sqrt{\frac{r_{p4}^2 + r_{p6}^2}{2}}\,,\quad r_{p2} = \sqrt{\frac{r_{p1}^2 + r_{p3}^2}{2}}\,,\ \text{and}\ \ r_{p0} = \frac{r_{p1}}{\sqrt{2}}\ . \tag{4-117}$$

The heat-transfer coefficients for the cladding and the pin/control surface are

$$h_{S4} = \frac{\kappa_s}{r_{p6}\ln\left(r_{p6}/r_{p5}\right)}\ \text{ and }\ h_{S1/S9} = \frac{\kappa_{f/cnt}}{r_{p3}\ln\left(r_{p3}/r_{p2}\right)}\ . \tag{4-118}$$

The heat-transfer coefficients between the cladding and the pin fuel/control and between pin fuel/control surface node and interior node are given by

$$h_{S1/S9,S4} = \left[\frac{r_{p3}}{\kappa_{f/cnt}}\ln\left(\frac{r_{p3}}{r_{p2}}\right) + \frac{1}{h_{GAP}} + \frac{r_{p4}}{\kappa_s}\ln\left(\frac{r_{p5}}{r_{p4}}\right)\right]^{-1}\ \text{, and} \tag{4-119}$$

$$h_{\mathrm{int},S1/S9} = \frac{\kappa_{f/c}}{r_{p1}\left[\ln\left(r_{p1}/r_{p0}\right) + \ln\left(r_{p2}/r_{p1}\right)\right]}\ , \tag{4-120}$$

where h_{GAP} represents the gap conductance and given by the input constant.

A typical value of 5678.26W/m^2/K is adopted tentatively as the default value. However, it is obvious that the fuel pellet expands depending on the temperature in the accident condition. Thus, the following two mechanistic models are available optionally.

The first model is simply to evaluate thermal expansion of fuel pellet by re-defining each radius of r_{p3} and r_{p4} taking the volume fraction of fuel into account. That is

$$h_{GAP} = \max\left\{h_{GAP,\min}, \min\left[h_{GAP,\max}, \frac{\kappa_{gas}}{r_{p4}\ln\left(r_{p4}/r_{p3}\right)}\right]\right\}, \tag{4-121}$$

where $h_{GAP,\min}$ and $h_{GAP,\max}$ are minimum and maximum values, respectively, of the gap

conductance. κ_{gas} is the gap thermal conductivity which is defined on one hand as an input constant (default value: 0.511043W/m/K) or on the other hand as a fission gas thermal conductivity given by EOS function at an average temperature between the pin fuel surface and the cladding.

The second model is represented by

$$h_{GAP} = \max\left\{h_{GAP,\min}, \min\left[h_{GAP,\max}, \left(h_{GAP,cond} + h_{GAP,rad}\right)\right]\right\} , \tag{4-122}$$

where $h_{GAP,\min}$ and $h_{GAP,\max}$ are minimum and maximum values, respectively, of the gap conductance. $h_{GAP,cond}$ is the model of originally proposed by Ross and Stoute. That is

$$h_{GAP,cond} = \frac{\kappa_{gas}}{C_{GAP} + g_{GAP} + r_{p4}\ln\left(r_{p4}/r_{p3}\right)} , \tag{4-123}$$

where C_{GAP} relating to the surface roughness of fuel and cladding is a constant fitting parameter of 2.01×10^{-4}. g_{GAP} stands for the following total jump distance of fuel and cladding:

$$g_{GAP} = 1373\left(\frac{2-a}{a}\right)\left(\frac{\kappa_{gas}\sqrt{T_{gas}w_5}}{P_{GAP}}\right) , \tag{4-124}$$

where κ_{gas} and T_{gas} represent respectively a fission gas thermal conductivity given by EOS function and an average temperature between pin fuel surface and cladding. P_{GAP} is here a constant value of 3.87×10^{5} [Pa] as the gap pressure. w_5 is the molecular weight of fission gas. a is given using A_1=0.812, A_2=4.52 and A_3=7.71 by

$$a = A_1\exp\left\{-\left(\ln(w_5) - A_2\right)^2 \Big/ A_3\right\} . \tag{4-125}$$

$h_{GAP,rad}$ is the term with radiation heat transfer. Since the radiation heat transfer between the fuel and the cladding can be treated as a set of finite parallel plates, the following equation can be adopted. That is

$$h_{GAP,rad} = \frac{\sigma_{SB}}{1/\varepsilon_f + 1/\varepsilon_c - 1}\frac{T_f^4 - T_c^4}{T_f - T_c} . \tag{4-126}$$

where σ_{SB} is the Stefan-Boltzmann constant (5.67×10^{-8} W/m^2/K^4). T_f and T_c are

temperature of pin fuel surface and cladding, respectively. ε_f and ε_c represent the emissivity of fuel and cladding, respectively, default values of which are 0.9 and 0.18.

The pin surface area is assumed to be proportional to the initial value and the transient change in volume is taken into account. When the structure volume fraction, which is defined in Section4.4, is smaller than 0.9, the increase in the pin volume increases the pin surface area because multiple pins do not contact each other. On the other hand, as the structure volume fraction is increased above 0.9, multiple pins come into contact and then the surface area decreases. This algorithm is formulated to determine the pin surface area by

$$a_{PIN} = a^i_{PIN}\,\zeta\sqrt{\frac{\alpha_{PIN}}{\alpha^i_{PIN}}} \quad \text{, where } \zeta = 1 \text{ for } \alpha_S \le 0.9 \quad \text{, and} \tag{4-127}$$

$$\zeta = \left[10(1-\alpha_S)\right]^{1/2} \quad \text{for } \alpha_S > 0.9 \ . \tag{4-128}$$

The pin surface area approaches to zero as the structure volume fraction approaches to one, and the pin-to-fluid contact area becomes smaller.

The structure-side heat-transfer coefficient is given by

$$h_{k1} = h_{S4} \quad \text{, for } h_{S4} \le \frac{\overline{\rho}_{s7} c_{S4}}{\Delta t a_{pin}} \quad \text{, and} \tag{4-129}$$

$$h_{k1} = h_{S1/S9,S4} \quad \text{, for } h_{S4} > \frac{\overline{\rho}_{s7} c_{S4}}{\Delta t a_{pin}} \ . \tag{4-130}$$

(2) Case 2 (only pin fuel/control without cladding)

This is the case where there is no cladding in Case 1. Therefore, heat-transfer coefficients and surface area are given as same as Case 1. The structure-side heat-transfer coefficient is given by

$$h_{k1} = \min\left[h_{S1}, \frac{(\rho_{s1}+\rho_{s2})c_{S1}}{\Delta t a_{pin}}\right] \quad \text{or} \quad h_{k1} = \min\left[h_{S9}, \frac{\rho_{s12} c_{S9}}{\Delta t a_{pin}}\right]. \tag{4-131}$$

(3) Case 3 (only cladding without pin fuel/control)

Case 3a is the special case where there is no pin fuel/control in Case 1. Case 3b is the case with no non-flow volume in Case 3a. Therefore, heat-transfer coefficients and surface area for each case are given as same as Case 1. The heat transfer coefficient of

the structure side is given by

$$h_{k1} = \min\left[h_{S4}, \frac{\overline{\rho}_{s7} c_{S4}}{\Delta t a_{pin}} \right], \text{ where } \; r_{p5} = r_{p6} \big/ \sqrt{2} \;\; \text{for Case 3b.} \tag{4-132}$$

4.4. Structure Volume Fraction

After defining all the structure configurations for can walls and fuel pin, the total structure volume fraction is calculated in the EOS routine by

$$\begin{aligned}
\alpha_S = {} & \alpha_{\text{int}} + [\overline{\rho}_{s1} + \overline{\rho}_{s2}] v_{S1} + [\overline{\rho}_{s3} + \overline{\rho}_{s4}] v_{S2} + [\overline{\rho}_{s5} + \overline{\rho}_{s6}] v_{S3} + \overline{\rho}_{s7} v_{S4} + \overline{\rho}_{s12} v_{S9} \\
& + \overline{\rho}_{s8}(ij) v_{S5}(ij) H[NCANL(ij)] + \overline{\rho}_{s9}(ij) v_{S6}(ij) \\
& + \overline{\rho}_{s10}(ij) v_{S7}(ij) H[NCANR(ij)] + \overline{\rho}_{s11}(ij) v_{S8}(ij) \\
& + \overline{\rho}_{s8}(ij+1) v_{S5}(ij+1) H[1 - NCANL(ij+1)] \frac{V_{ij+1}}{V_{ij}} \\
& + \overline{\rho}_{s10}(ij-1) v_{S7}(ij-1) H[1 - NCANR(ij-1)] \frac{V_{ij-1}}{V_{ij}} \\
& + \alpha_{nf,PIN} + \alpha_{nf,LCW} + \alpha_{nf,RCW} \;\; ,
\end{aligned} \tag{4-133}$$

where $H(x)$ is the Heaviside function which is

$H(x) = 1$, if $x > 0$, and

$H(x) = 0$,if $x \le 0$.

The variables of NCANL and NCANR are defined in Section 4.2.1.

The first four terms denote the volume fractions of pin fuel including an interior node, left and right crust fuels in cell *ij*. The calculation of can wall volume fractions requires rather complex formulation. As discussed in Section 4.2.2, the macroscopic density of a can wall surface node in a cell may be taken from the adjacent cell when the two cells are coupled. This surface node must be taken back to the original cell to conserve the structure volume fraction and the flow area. As already noted, the cell volume ratio is multiplied to conserve mass. Equation (4-133) thus contains the logic of set-over of can wall surface nodes. The volume fraction of flow is a crucial variable in SIMMER-III and is defined as $(1 - \alpha_S)$.

4.5. Hydraulic Diameter

All the structure configurations for can walls and fuel pin, and the structure volume fraction are defined in the previous sections. Then the hydraulic diameter can be determined for each cell. The general definition is given by

$$D_h = \frac{4\times[\text{Flow area}]}{[\text{wetted perimeter}]} = \frac{4A_{flow}}{P_{wet}} \quad . \tag{4-134}$$

The flow area and wetted perimeter per unit volume are calculated by

$$A_{flow} = [1-\alpha_S]/V \quad \text{, and} \tag{4-135}$$

$$P_{wet} = [a_{pin} + a_{LCW} + a_{RCW}]/V \text{ , respectively.} \tag{4-136}$$

Thus the hydraulic diameter is defined by

$$D_h = \frac{4(1-\alpha_S)}{a_{pin} + a_{LCW} + a_{RCW}} \quad , \tag{4-137}$$

where a_{pin}, a_{LCW} and a_{RCW} are the structure surface areas per unit volume as calculated in the previous sections. When there is no structure existing in a cell, the hydraulic diameter is set to a large value of 1×10^{20} or is defined based on a mesh-cell width as ΔR an option.

$$D_h = 4(1-\alpha_S)\Delta R \quad . \tag{4-138}$$

Additional consideration has to be made about the definition of the hydraulic diameter in a large pool configuration with an outer wall. Based on the above definition, the diameter in cells with no structure is set to a large value, whilst the diameter in cells with wall is determined from the structure volume fraction. Since the structure volume fraction α_S is dependent on a cell volume, the diameter becomes mesh-cell-size dependent and hence rather arbitrary. Because of this inconvenience, an option is also available to explicitly define the hydraulic diameter by user input.

It is also noted that the selection of flow regimes, pool or channel, in a mesh cell is determined from the hydraulic diameter. If the hydraulic diameter D_h is larger than the input threshold denoted by $D_{h,pool}$, then the flow in the cell is regarded as “pool flow”. On the other hand, if $D_h \le D_{h,pool}$, the cell is considered to be a channel flow.

The input threshold is defaulted to $D_{h,pool} = 1.0$, and the user can select the flow regime by specifying the input hydraulic diameter arbitrarily.

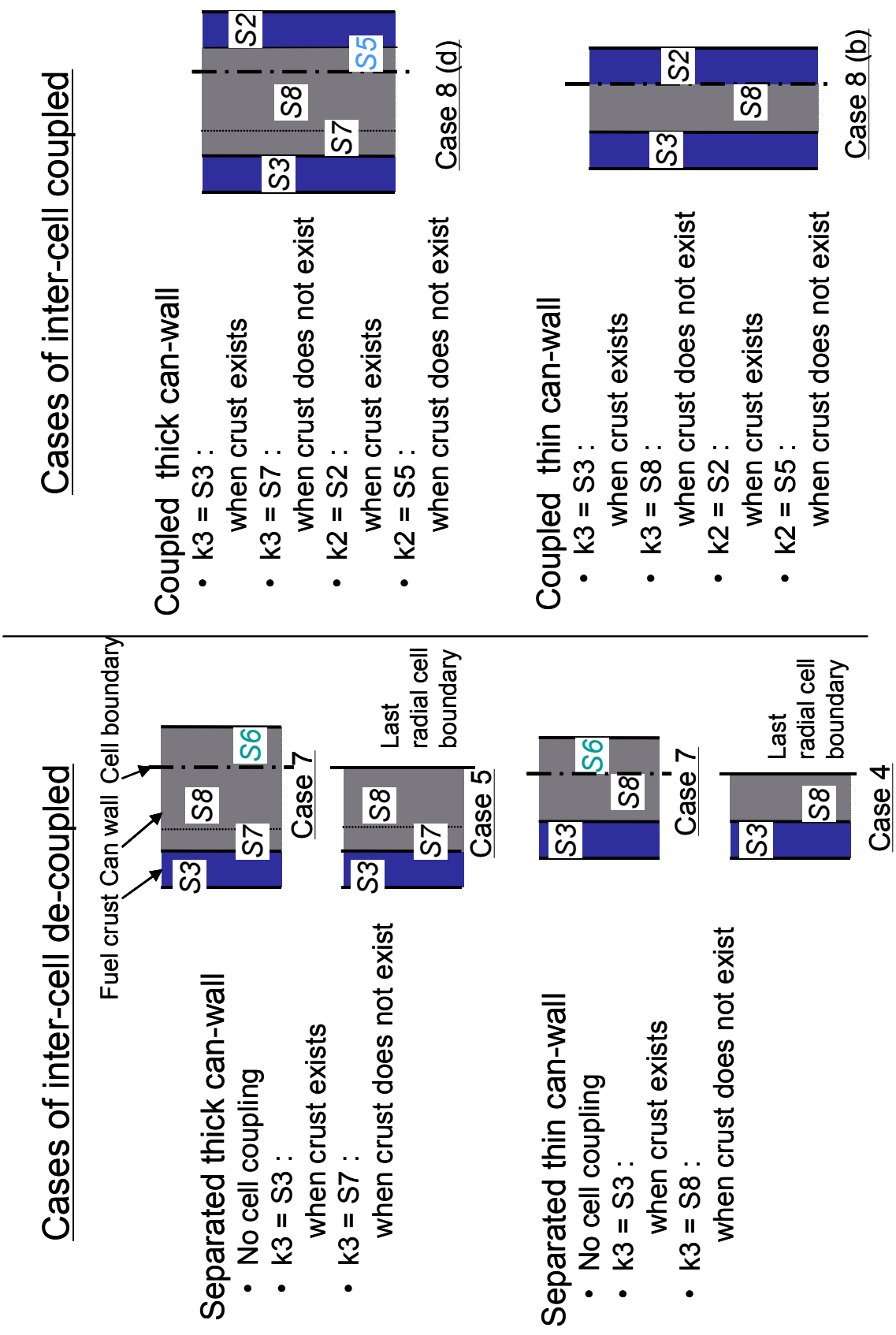

Fig. 4-1 Can-Wall Configurations (Examples for right cell boundary)

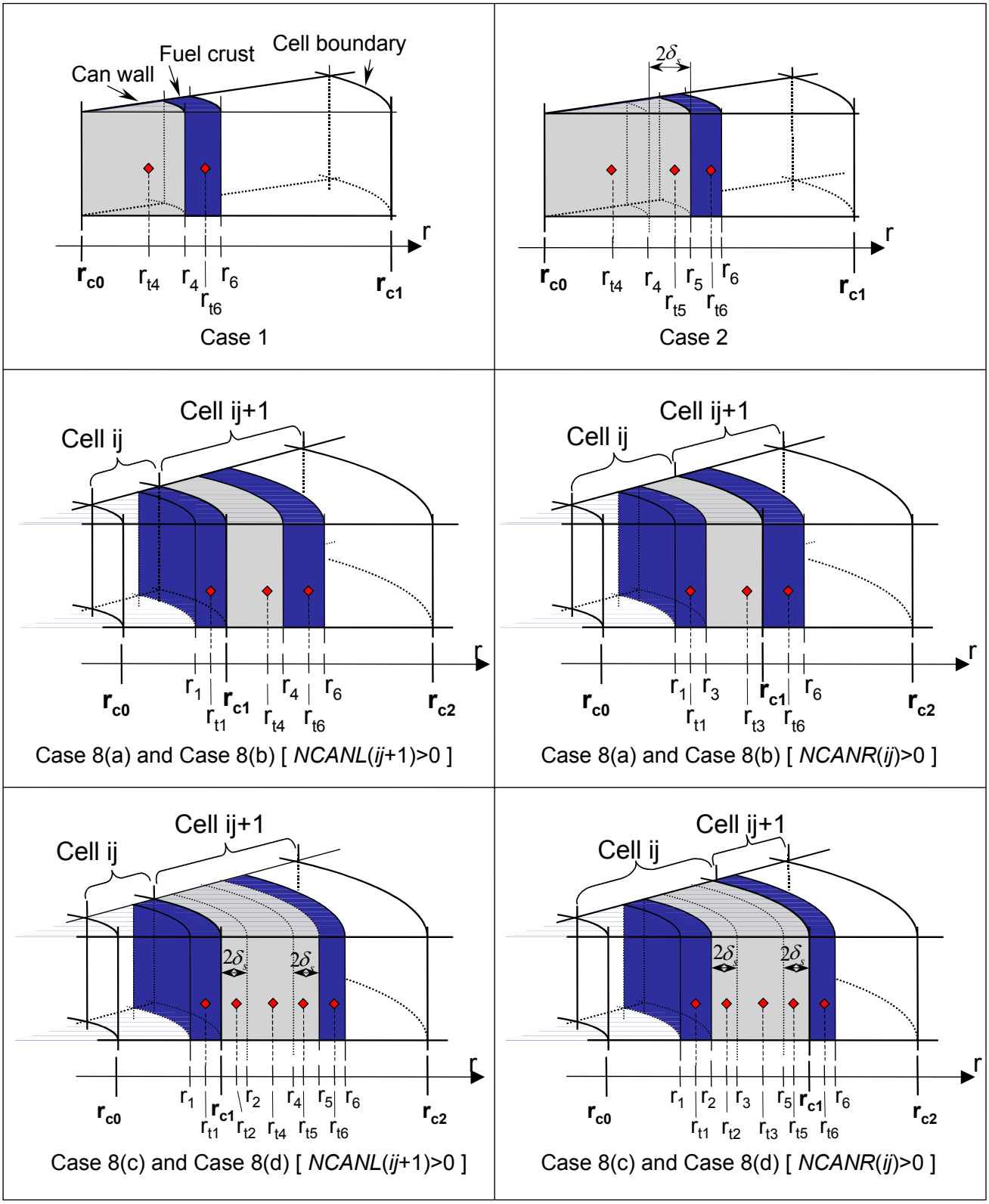

Fig.4-2 Each Radius of Node Boundaries and Temperature Points for Can Wall in the Cylindrical Geometry.

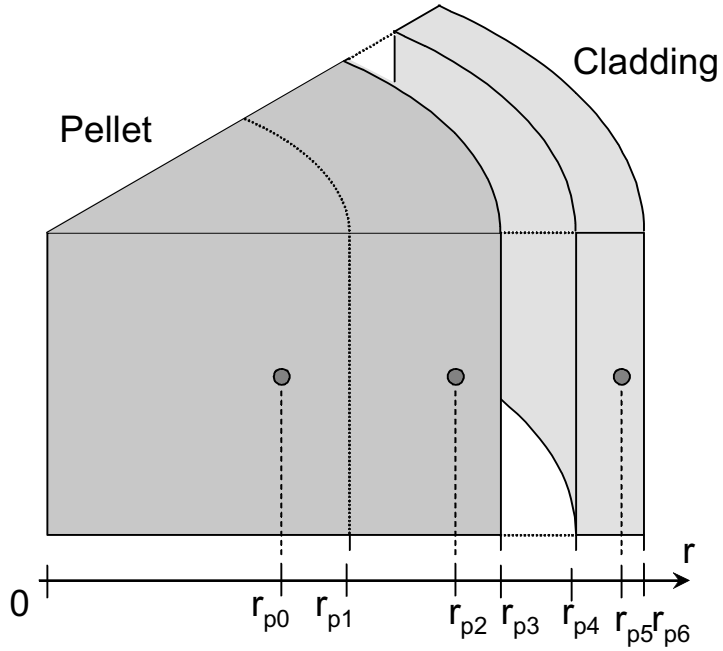

Fig. 4-3 Each Radius of Node Boundaries and Temperature Points for Fuel Pin.

5. Can Wall Heat-Transfer Model

5.1. Overview of Can Wall Heat-Transfer Model

Among the various modes of heat and mass transfer associated with the structure, the can wall heat-transfer model is described in this section. Crust fuel coupled with the structure is also treated. Since the heat and mass transfer between the structure surface and fluid, including non-equilibrium melting/freezing is modeled in fluid dynamics in the reference 11, only the heat conduction inside the can wall is treated here. A thin can wall without crust fuel need not be treated because there is only one node in this case.

Three apparent situations are considered as follows:

(1) An isolated can wall with or without crust, where the can wall has thermal contact within one cell;

(2) A thin can wall coupled with an adjacent cell, in which crust fuel should exist; and

(3) A thick can wall coupled with an adjacent cell, with or without crust.

In this section, the model only for the left can wall is described, and the same formations are applicable to the right can wall by replacing the subscripts of right components with those of left components. In addition, only the model for the slab geometry is described here, because the same formations are applicable by replacing constant structure-structure heat-transfer areas (a_{LCW}) to those of the cylindrical geometries ($a_{Sm,Sn}$) which depend on configurations as described in Section 4.2.

5.2. Isolated Can Wall

A single isolated can wall is represented by one or two nodes depending on the thickness. There are three cases to be modeled in this section.

5.2.1. Case 1 (thick can wall without crust)

There are two can wall nodes, interior and surface, in this case. The can wall surface node is in contact with fluid and the fluid-structure transfers have updated the macroscopic density and specific internal energy of the surface node. Then the differential equations are written as

$$\frac{\partial \overline{\rho}_{s8} e_{S5}}{\partial t} = a_{LCW} h_{S5,S6} \left(\tilde{T}_{S6}^{n+1} - \tilde{T}_{S5}^{n+1} \right) \text{, and} \tag{5-1}$$

$$\frac{\partial \overline{\rho}_{s9} e_{S6}}{\partial t} = - \frac{\partial \overline{\rho}_{s8} e_{S5}}{\partial t} . \tag{5-2}$$

5.2.2. Case 2 (thin can wall with crust)

In this case, the can wall is modeled by a single interior node. The similar formulation is applicable as Case 1, by replacing the can wall surface node with crust. Thus, the differential equations are written as

$$\frac{\partial (\overline{\rho}_{s3} + \overline{\rho}_{s4}) e_{S2}}{\partial t} = a_{LCW} h_{S2,S6} \left(\tilde{T}_{S6}^{n+1} - \tilde{T}_{S2}^{n+1} \right) = - \frac{\partial \overline{\rho}_{s9} e_{S6}}{\partial t} . \tag{5-3}$$

5.2.3. Case 3 (thick can wall with crust)

A three-node heat-transfer formation is given by

$$\frac{\partial (\overline{\rho}_{s3} + \overline{\rho}_{s4}) e_{S2}}{\partial t} = a_{LCW} h_{S2,S5} \left(\tilde{T}_{S5}^{n+1} - \tilde{T}_{S2}^{n+1} \right) , \tag{5-4}$$

$$\frac{\partial \overline{\rho}_{s9} e_{S6}}{\partial t} = a_{LCW} h_{S5,S6} \left(\tilde{T}_{S5}^{n+1} - \tilde{T}_{S6}^{n+1} \right) \text{, and} \tag{5-5}$$

$$\frac{\partial \overline{\rho}_{s8} e_{S5}}{\partial t} = - \frac{\partial (\overline{\rho}_{s3} + \overline{\rho}_{s4}) e_{S2}}{\partial t} - \frac{\partial \overline{\rho}_{s9} e_{S6}}{\partial t} . \tag{5-6}$$

5.2.4. Solution procedure

In this isolated can wall situation, there are two different types of equations. In Cases 1 and 2, a set of two coupled equations with two unknowns are written of the form,

$$\frac{\partial \overline{\rho}_1 e_1}{\partial t} = a h_{1,2} \left(\tilde{T}_2^{n+1} - \tilde{T}_1^{n+1} \right) \text{ , and} \tag{5-7}$$

$$\frac{\partial \overline{\rho}_2 e_2}{\partial t} = a h_{1,2} \left(\tilde{T}_1^{n+1} - \tilde{T}_2^{n+1} \right) . \tag{5-8}$$

Case 3 represents a set of three coupled equations with three unknowns of the form,

$$\frac{\partial \overline{\rho}_1 e_1}{\partial t} = a h_{1,2} \left(\tilde{T}_2^{n+1} - \tilde{T}_1^{n+1} \right) , \tag{5-9}$$

$$\frac{\partial \overline{\rho}_2 e_2}{\partial t} = ah_{1,2}\left(\tilde{T}_1^{n+1} - \tilde{T}_2^{n+1}\right) + ah_{2,3}\left(\tilde{T}_3^{n+1} - \tilde{T}_2^{n+1}\right) \text{ , and} \tag{5-10}$$

$$\frac{\partial \overline{\rho}_3 e_3}{\partial t} = ah_{2,3}\left(\tilde{T}_2^{n+1} - \tilde{T}_3^{n+1}\right) \quad . \tag{5-11}$$

These formulations are implicit, since the temperatures appearing on the right side are the end-of-time-step values. In both the types, the end-of-time-step temperatures are estimated by expanding in a Taylor series as

$$\tilde{T}_{Sm}^{n+1} = T_{Sm}^{n} + \left(\frac{\partial T_{Sm}}{\partial e_{Sm}}\right)^n \Delta e_{Sm} \quad . \tag{5-12}$$

Then, because the densities remain constant, Eqs. (5-7) - (5-8) are re-written in finite-difference form,

$$\left[\overline{\rho}_1 + (ah)_{1,2}\Delta t \frac{\partial T_1}{\partial e_1}\right]\Delta e_1 - \left[(ah)_{1,2}\Delta t \frac{\partial T_2}{\partial e_2}\right]\Delta e_2 = (ah)_{1,2}\Delta t\left(T_2^n - T_1^n\right), \text{ and} \tag{5-13}$$

$$-\left[(ah)_{1,2}\Delta t \frac{\partial T_1}{\partial e_1}\right]\Delta e_1 + \left[\overline{\rho}_2 + (ah)_{1,2}\Delta t \frac{\partial T_2}{\partial e_2}\right]\Delta e_2 = (ah)_{1,2}\Delta t\left(T_1^n - T_2^n\right) \quad . \tag{5-14}$$

These are two linear equations in two unknowns from which the Δe_1 and Δe_2 can be determined easily.

Similarly, using Eq. (5-12), Eqs. (5-9) - (5-11) in finite-difference form are

$$\left[\overline{\rho}_1 + (ah)_{1,2}\Delta t \frac{\partial T_1}{\partial e_1}\right]\Delta e_1 - \left[(ah)_{1,2}\Delta t \frac{\partial T_2}{\partial e_2}\right]\Delta e_2 = (ah)_{1,2}\Delta t\left(T_2^n - T_1^n\right) \text{ ,} \tag{5-15}$$

$$-\left[(ah)_{1,2}\Delta t \frac{\partial T_1}{\partial e_1}\right]\Delta e_1 + \left[\overline{\rho}_2 + \left\{(ah)_{1,2} + (ah)_{2,3}\right\}\Delta t \frac{\partial T_2}{\partial e_2}\right]\Delta e_2 + \left[(ah)_{2,3}\Delta t \frac{\partial T_3}{\partial e_3}\right]\Delta e_3$$

$$= \Delta t\left[(ah)_{1,2}\left(T_1^n - T_2^n\right) + (ah)_{2,3}\left(T_3^n - T_2^n\right)\right] \text{ , and} \tag{5-16}$$

$$-\left[(ah)_{2,3}\Delta t \frac{\partial T_2}{\partial e_2}\right]\Delta e_2 + \left[\overline{\rho}_3 + (ah)_{2,3}\Delta t \frac{\partial T_3}{\partial e_3}\right]\Delta e_3 = (ah)_{2,3}\Delta t\left(T_2^n - T_3^n\right) \quad . \tag{5-17}$$

Equations from (5-15) to (5-17) form three linear equations to determine Δe_1, Δe_2 and Δe_3. Specific internal energies are simply updated by

$$\tilde{e}_{Sm}^{n+1} = e_{Sm}^{n} + \Delta e_{Sm} \quad . \tag{5-18}$$

Here, it is assumed that the time step in the fluid-dynamics step is sufficiently small that no iteration is to be performed.

5.3. Thin Can Wall Contacting an Adjacent Cell

A thin can wall is represented by a single interior node. In this situation, crust must exist; otherwise, no heat-transfer calculation is required. There are three cases depending on where the crust exists.

5.3.1. Case 1 (crust in the can wall cell)

In this case, the adjacent cell does not possess a crust and there is a crust in the cell where the can wall exists. This case is exactly the same as Case 2 in Section 5.2, and hence equations need not be re-written.

5.3.2. Case 2 (crust in the adjacent cell)

In this case, crust only exists in the adjacent cell. The differential equations should be

$$\left[\frac{\partial(\overline{\rho}_{s5}+\overline{\rho}_{s6})e_{S3}}{\partial t}\right]_{ij-1} = (ha)_{S3(ij-1),S6(ij)}\left(\tilde{T}_{S6(ij)}^{n+1} - \tilde{T}_{S3(ij-1)}^{n+1}\right) \text{ , and} \tag{5-19}$$

$$\left[\frac{\partial\overline{\rho}_{s9}e_{S6}}{\partial t}\right]_{ij} = -\left[\frac{\partial(\overline{\rho}_{s5}+\overline{\rho}_{s6})e_{S3}}{\partial t}\right]_{ij-1} . \tag{5-20}$$

5.3.3. Case 3 (crust in both the cells)

In this case, there are crusts in the adjacent cell and the cell where the can wall exists. Then, the differential equations should be

$$\left[\frac{\partial(\overline{\rho}_{s3}+\overline{\rho}_{s4})e_{S2}}{\partial t}\right]_{ij} = \left(h_{S2,S6}a_{LCW}\right)_{ij}\left(\tilde{T}_{S6(ij)}^{n+1} - \tilde{T}_{S2(ij)}^{n+1}\right) \quad , \tag{5-21}$$

$$\left[\frac{\partial(\overline{\rho}_{s5}+\overline{\rho}_{s6})e_{S3}}{\partial t}\right]_{ij-1} = (ha)_{S3(ij-1),S6(ij)}\left(\tilde{T}_{S6(ij)}^{n+1} - \tilde{T}_{S3(ij-1)}^{n+1}\right) \text{ , and} \tag{5-22}$$

$$\left[\frac{\partial\overline{\rho}_{s9}e_{S6}}{\partial t}\right]_{ij} = -\left[\frac{\partial(\overline{\rho}_{s5}+\overline{\rho}_{s6})e_{S3}}{\partial t}\right]_{ij-1} - \left[\frac{\partial(\overline{\rho}_{s3}+\overline{\rho}_{s4})e_{S2}}{\partial t}\right]_{ij} . \tag{5-23}$$

5.3.4. Solution procedure

The equations in Cases 1 and 2 form a set of coupled two equations, and the equations in Case 3 form a set of coupled three equations. Therefore, the same solution procedure as described in Section 5.2 is applicable. It is noted that the macroscopic densities of the crust fuel in the adjacent cell must be multiplied by the cell volume ratio in Case 2 and 3 to conserve the total energy, because the macroscopic densities are cell volume dependent variables.

5.4. Thick Can Wall Contacting an Adjacent Cell

In this situation, the thick can wall has two surface nodes on both sides. Therefore, there are four cases depending on whether or not and where the crust exists.

5.4.1. Case 1 (without crust)

There is no crust in this case, therefore three structure components exist. The differential equations should be

$$\left[\frac{\partial \overline{\rho}_{s10} e_{S7}}{\partial t}\right]_{ij-1} = (ha)_{S7(ij-1),S6(ij)}\left(\tilde{T}^{n+1}_{S6(ij)} - \tilde{T}^{n+1}_{S7(ij-1)}\right) \quad , \tag{5-24}$$

$$\left[\frac{\partial \overline{\rho}_{s9} e_{S6}}{\partial t}\right]_{ij} = -\left[\frac{\partial \overline{\rho}_{s10} e_{S7}}{\partial t}\right]_{ij-1} - \left[\frac{\partial \overline{\rho}_{s8} e_{S5}}{\partial t}\right]_{ij} \quad \text{, and} \tag{5-25}$$

$$\left[\frac{\partial \overline{\rho}_{s8} e_{S5}}{\partial t}\right]_{ij} = \left(h_{S5,S6} a_{LCW}\right)_{ij}\left(\tilde{T}^{n+1}_{S6(ij)} - \tilde{T}^{n+1}_{S5(ij)}\right) \quad . \tag{5-26}$$

5.4.2. Case 2 (crust in the adjacent cell)

In this case, the crust exists only in the adjacent cell, and hence four structure components exist. The differential equations should be

$$\left[\frac{\partial (\overline{\rho}_{s5} + \overline{\rho}_{s6}) e_{S3}}{\partial t}\right]_{ij-1} = \left(h_{S3,S7} a_{RCW}\right)_{ij-1}\left(\tilde{T}^{n+1}_{S7(ij-1)} - \tilde{T}^{n+1}_{S3(ij-1)}\right) \quad , \tag{5-27}$$

$$\left[\frac{\partial \overline{\rho}_{s10} e_{S7}}{\partial t}\right]_{ij-1} = -\left[\frac{\partial (\overline{\rho}_{s5} + \overline{\rho}_{s6}) e_{S3}}{\partial t}\right]_{ij-1} + (ha)_{S7(ij-1),S6(ij)}\left(\tilde{T}^{n+1}_{S6(ij)} - \tilde{T}^{n+1}_{S7(ij-1)}\right) \quad , \tag{5-28}$$

$$\left[\frac{\partial \overline{\rho}_{s9} e_{S6}}{\partial t}\right]_{ij} = (ha)_{S7(ij-1),S6(ij)}\left(\tilde{T}^{n+1}_{S7(ij-1)} - \tilde{T}^{n+1}_{S6(ij)}\right) - \left[\frac{\partial \overline{\rho}_{s8} e_{S5}}{\partial t}\right]_{ij} \quad \text{, and} \tag{5-29}$$

$$\left[\frac{\partial \overline{\rho}_{s8} e_{S5}}{\partial t}\right]_{ij} = \left(h_{S5,S6} a_{LCW}\right)_{ij} \left(\widetilde{T}^{n+1}_{S6(ij)} - \widetilde{T}^{n+1}_{S5(ij)}\right) \quad . \tag{5-30}$$

5.4.3. Case 3 (crust in the cell)

In this case, crust exists only in the cell where the can wall interior node is present, and hence four structure components exist. The differential equations should be

$$\left[\frac{\partial \overline{\rho}_{s10} e_{S7}}{\partial t}\right]_{ij-1} = \left(ha\right)_{S7(ij-1),S6(ij)} \left(\widetilde{T}^{n+1}_{S6(ij)} - \widetilde{T}^{n+1}_{S7(ij-1)}\right) \quad , \tag{5-31}$$

$$\left[\frac{\partial \overline{\rho}_{s9} e_{S6}}{\partial t}\right]_{ij} = -\left[\frac{\partial \overline{\rho}_{s10} e_{S7}}{\partial t}\right]_{ij-1} + \left(h_{S5,S6} a_{LCW}\right)_{ij} \left(\widetilde{T}^{n+1}_{S5(ij)} - \widetilde{T}^{n+1}_{S6(ij)}\right) \quad , \tag{5-32}$$

$$\left[\frac{\partial \overline{\rho}_{s8} e_{S5}}{\partial t}\right]_{ij} = \left(h_{S5,S6} a_{LCW}\right)_{ij} \left(\widetilde{T}^{n+1}_{S6(ij)} - \widetilde{T}^{n+1}_{S5(ij)}\right) - \left[\frac{\partial \left(\overline{\rho}_{s3} + \overline{\rho}_{s4}\right) e_{S2}}{\partial t}\right]_{ij} \quad \text{, and} \tag{5-33}$$

$$\left[\frac{\partial \left(\overline{\rho}_{s3} + \overline{\rho}_{s4}\right) e_{S2}}{\partial t}\right]_{ij} = \left(h_{S2,S5} a_{LCW}\right)_{ij} \left(\widetilde{T}^{n+1}_{S5(ij)} - \widetilde{T}^{n+1}_{S2(ij)}\right) \quad . \tag{5-34}$$

5.4.4. Case 4 (crusts on two cells)

In this case, there are two crust components on both the surface nodes of the thick can wall, and hence five structure components exist. The differential equations should be

$$\left[\frac{\partial \left(\overline{\rho}_{s5} + \overline{\rho}_{s6}\right) e_{S3}}{\partial t}\right]_{ij-1} = \left(h_{S3,S7} a_{RCW}\right)_{ij-1} \left(\widetilde{T}^{n+1}_{S7(ij-1)} - \widetilde{T}^{n+1}_{S3(ij-1)}\right) \quad , \tag{5-35}$$

$$\left[\frac{\partial \overline{\rho}_{s10} e_{S7}}{\partial t}\right]_{ij-1} = -\left[\frac{\partial \left(\overline{\rho}_{s5} + \overline{\rho}_{s6}\right) e_{S3}}{\partial t}\right]_{ij-1} + \left(ha\right)_{S7(ij-1),S6(ij)} \left(\widetilde{T}^{n+1}_{S6(ij)} - \widetilde{T}^{n+1}_{S7(ij-1)}\right) \quad , \tag{5-36}$$

$$\left[\frac{\partial \overline{\rho}_{s9} e_{S6}}{\partial t}\right]_{ij} = \left(ha\right)_{S7(ij-1),S6(ij)} \left(\widetilde{T}^{n+1}_{S7(ij-1)} - \widetilde{T}^{n+1}_{S6(ij)}\right) + \left(h_{S5,S6} a_{LCW}\right)_{ij} \left(\widetilde{T}^{n+1}_{S5(ij)} - \widetilde{T}^{n+1}_{S6(ij)}\right), \tag{5-37}$$

$$\left[\frac{\partial \overline{\rho}_{s8} e_{S5}}{\partial t}\right]_{ij} = \left(h_{S5,S6} a_{LCW}\right)_{ij} \left(\widetilde{T}^{n+1}_{S6(ij)} - \widetilde{T}^{n+1}_{S5(ij)}\right) - \left[\frac{\partial \left(\overline{\rho}_{s3} + \overline{\rho}_{s4}\right) e_{S2}}{\partial t}\right]_{ij} \quad \text{, and} \tag{5-38}$$

$$\left[\frac{\partial \left(\overline{\rho}_{s3} + \overline{\rho}_{s4}\right) e_{S2}}{\partial t}\right]_{ij} = \left(h_{S2,S5} a_{LCW}\right)_{ij} \left(\widetilde{T}^{n+1}_{S5(ij)} - \widetilde{T}^{n+1}_{S2(ij)}\right) \quad . \tag{5-39}$$

5.4.5. Solution procedure

The equations in Case 1 are of the form of equations in the previous sections; therefore the same solution procedure is applicable by multiplying macroscopic density of the wall surface node in the adjacent cell taking the cell volume ratio into account. The equations in Cases 2 and 3 are four coupled equations of the form

$$\frac{\partial \overline{\rho}_1 e_1}{\partial t} = (ah)_{1,2}\left(\tilde{T}_2^{n+1} - \tilde{T}_1^{n+1}\right) \quad , \tag{5-40}$$

$$\frac{\partial \overline{\rho}_2 e_2}{\partial t} = (ah)_{1,2}\left(\tilde{T}_1^{n+1} - \tilde{T}_2^{n+1}\right) + (ah)_{2,3}\left(\tilde{T}_3^{n+1} - \tilde{T}_2^{n+1}\right) \quad , \tag{5-41}$$

$$\frac{\partial \overline{\rho}_3 e_3}{\partial t} = (ah)_{2,3}\left(\tilde{T}_2^{n+1} - \tilde{T}_3^{n+1}\right) + (ah)_{3,4}\left(\tilde{T}_4^{n+1} - \tilde{T}_3^{n+1}\right) \text{ , and} \tag{5-42}$$

$$\frac{\partial \overline{\rho}_4 e_4}{\partial t} = (ah)_{3,4}\left(\tilde{T}_3^{n+1} - \tilde{T}_4^{n+1}\right) \quad . \tag{5-43}$$

The equations in Case 4 are five coupled equations of the form

$$\frac{\partial \overline{\rho}_1 e_1}{\partial t} = (ah)_{1,2}\left(\tilde{T}_2^{n+1} - \tilde{T}_1^{n+1}\right) \quad , \tag{5-44}$$

$$\frac{\partial \overline{\rho}_2 e_2}{\partial t} = (ah)_{1,2}\left(\tilde{T}_1^{n+1} - \tilde{T}_2^{n+1}\right) + (ah)_{2,3}\left(\tilde{T}_3^{n+1} - \tilde{T}_2^{n+1}\right) \quad , \tag{5-45}$$

$$\frac{\partial \overline{\rho}_3 e_3}{\partial t} = (ah)_{2,3}\left(\tilde{T}_2^{n+1} - \tilde{T}_3^{n+1}\right) + (ah)_{3,4}\left(\tilde{T}_4^{n+1} - \tilde{T}_3^{n+1}\right) \quad , \tag{5-46}$$

$$\frac{\partial \overline{\rho}_4 e_4}{\partial t} = (ah)_{3,4}\left(\tilde{T}_3^{n+1} - \tilde{T}_4^{n+1}\right) + (ah)_{4,5}\left(\tilde{T}_5^{n+1} - \tilde{T}_4^{n+1}\right), \text{ and} \tag{5-47}$$

$$\frac{\partial \overline{\rho}_5 e_5}{\partial t} = (ah)_{4,5}\left(\tilde{T}_4^{n+1} - \tilde{T}_5^{n+1}\right) \quad . \tag{5-48}$$

It is noted that not only macroscopic densities but also structure-structure heat-transfer areas of the adjacent cell must be multiplied by the cell volume ratio, because heat-transfer areas are also cell volume dependent variables.

These sets of 4 or 5 differential equations form a standard tri-diagonal system with a

typical equation of the form

$$\left[\frac{\partial \overline{\rho}_m e_m}{\partial t}\right] = (ha)_{m-1.m}\left(\widetilde{T}_{m-1}^{n+1} - \widetilde{T}_m^{n+1}\right) + (ha)_{m.m+1}\left(\widetilde{T}_{m+1}^{n+1} - \widetilde{T}_m^{n+1}\right) \quad . \tag{5-49}$$

Expanding the end-of-time-step temperatures using Eq. (5-12) produces

$$-\left[(ah)_{m-1,m}\Delta t\frac{\partial T_{m-1}}{\partial e_{m-1}}\right]\Delta e_{m-1} + \left[\overline{\rho}_m + \left\{(ah)_{m-1,m} + (ah)_{m,m+1}\right\}\Delta t\frac{\partial T_m}{\partial e_m}\right]\Delta e_m$$

$$-\left[(ah)_{m,m+1}\Delta t\frac{\partial T_{m+1}}{\partial e_{m+1}}\right]\Delta e_{m+1} = \Delta t\left[(ah)_{m-1,m}\left(T_{m-1}^n - T_m^n\right) + (ah)_{m,m+1}\left(T_{m+1}^n - T_m^n\right)\right], \tag{5-50}$$

which is one equation of a tri-diagonal linear system for Δe_m . Solution for Δe_m allows determination of $\widetilde{e}_m^{n+1}$ by

$$\widetilde{e}_m^{n+1} = e_m^n + \Delta e_m \quad . \tag{5-51}$$

6. Fuel Pin Heat-Transfer Model

6.1. Overview of Simplified Fuel Pin Model

The simplified fuel-pin heat-transfer model is described in this section. The model is made available for a standard use in SIMMER-III. The model represents the fuel pellet in two radial nodes, surface and interior, and the cladding in one node. Because evaluation of fuel temperature is important in fast reactor accidents, the heat-transfer calculation is performed implicitly using the end-of-time-step temperatures. Even though only the fuel-pin calculation is described in this section, the same solution method is also used to treat the control pin. The thermal calculation of fission gas plenum is also performed, but the solution procedure is explicit due to slow thermal response of gas.

The simplified pin model is coded outside the fluid-dynamics model that operates in small time step sizes. It is intended that the pin model can operate in different and larger time step sizes because of the two reasons. First, due to relatively large thermal inertia and loose connection with the external fluid, the pellet interior may not be coupled tightly with fluid. Second, since the simplified model is consistently programmed with the detailed model that requires more computer time, the computing cost of fuel-pin thermal calculations can be reasonably saved. From the practical point of view, the actual computer time required for the simplified pin model is negligibly small. Therefore an option is currently available to operate the model in the same time steps as the fluid dynamics.

The fuel-pin failure is currently modeled based only on thermal conditions of pin fuel and cladding as the results of heat-transfer calculations. However this is modeled not in the pin model but in the fluid dynamics, since the resultant mass transfers should be tightly coupled with fluid dynamics.

6.2. Fuel Pin Structure Configuration

The heat-transfer calculation is based on the structure configuration described in Section 4.3. Since the model is programmed outside the fluid dynamics, different indexes are used to denote three fuel-pin components as shown previously in Table 2-4:

a : pin fuel interior node,

b : pin fuel surface node, and

c : cladding

The macroscopic densities and specific internal energies of the above components have one by one correspondence with fluid-dynamics components:

$$\overline{\rho}_a = \overline{\rho}_{\text{int}} \ ; \ \overline{\rho}_b = \overline{\rho}_{s1} + \overline{\rho}_{s2} \ \text{ and } \ \overline{\rho}_c = \overline{\rho}_7 \ , \text{ and} \tag{6-1}$$

$$e_a = e_{\text{int}} ; \ e_b = e_{S1} \ \text{ and } \ e_c = e_{S4} \ , \tag{6-2}$$

where the subscript int denotes the energy component corresponding to the pin fuel interior node. The heat-transfer coefficients and areas per unit volume are defined based on the structure configuration model as described in Section 4.3.

$$h_{a,b} = h_{\text{int},S1} \ \text{ and } \ h_{b,c} = h_{S1,S4} \ , \text{ and} \tag{6-3}$$

$$a_{a,b} = a_{\text{int},S1} \ \text{ and } \ a_{b,c} = a_{S1,S4} \ . \tag{6-4}$$

For the fission gas plenum, they are

$$h_{FG,c} = h_{FG,S4} \text{ , and } \ a_{FG,c} = a_{FG,S4} \ . \tag{6-5}$$

For the control pin, the same definition is made.

6.3. Fuel Pin Heat Transfer

The basic equations of mass and energy conservation for fuel-pin heat-transfer calculations are described by

$$\frac{\partial \overline{\rho}_m}{\partial t} = \Gamma_m \ , \text{ and} \tag{6-6}$$

$$\frac{\partial \overline{\rho}_m e_m}{\partial t} = h_{m,m-1} a_{m.m-1} \left(T_{m-1} - T_m\right) + h_{m+1,m} a_{m+1.m} \left(T_{m+1} - T_m\right) + Q_{Hm} + Q_{Nm} \ , \tag{6-7}$$

where the subscript m denotes one of the three fuel pin radial nodes. The mass-transfer rate, Γ_m , on the right hand side of Eq. (6-6) accounts for all the mode of mass transfers with fluid. Larger time step sizes can be used for pin heat transfer calculation and hence the mass-transfer rates calculated in the fluid dynamics are summed over several time steps included in the current heat-transfer time step. The Q_{Hm} and Q_{Nm} terms in Eq. (6-7) denote the energy transfer rates due to heat transfer

from fluid and nuclear heating, respectively. These are also summed over the several fluid-dynamics time steps included in the current heat-transfer step.

Equations (6-6) and (6-7) are finite-differenced implicitly using the end-of-time-step temperatures as

$$\tilde{\bar{\rho}}_m^{n+1} - \bar{\rho}_m^n = \Delta t \Gamma_m \quad \text{, and} \tag{6-8}$$

$$\tilde{\bar{\rho}}_m^{n+1}\tilde{e}_m^{n+1} - \bar{\rho}_m^n e_m^n =$$

$$\Delta t\left[h_{m,m-1}a_{m.m-1}\left(\tilde{T}_{m-1}^{n+1} - \tilde{T}_m^{n+1}\right) + h_{m+1,m}a_{m+1.m}\left(\tilde{T}_{m+1,m}^{n+1} - \tilde{T}_m^{n+1}\right) + Q_{Hm} + Q_{Nm}\right] \tag{6-9}$$

where the superscript n denotes the heat-transfer time step number, which is different from the fluid dynamics. From the above two equations, $\tilde{\bar{\rho}}_m^{n+1}$ is eliminated to form

$$\bar{\rho}_m^n\left[\tilde{e}_m^{n+1} - e_m^n\right] =$$

$$\Delta t\left[h_{m,m-1}a_{m,m-1}\left(\tilde{T}_{m-1}^{n+1} - \tilde{T}_m^{n+1}\right) + h_{m+1,m}a_{m+1,m}\left(\tilde{T}_{m+1}^{n+1} - \tilde{T}_m^{n+1}\right) + Q_{Hm} + Q_{Nm} - \Gamma_m\tilde{e}_m^{n+1}\right] \quad . \tag{6-10}$$

Then the end-of-time-step temperatures and specific internal energies are expanded with respect to the change in internal energies as

$$\tilde{T}_m^{n+1} = T_m^n + \left(\frac{\partial T_{Sm}}{\partial e_{Sm}}\right)^n \Delta e_m \quad \text{, and} \tag{6-11}$$

$$\tilde{e}_m^{n+1} = e_m^n + \Delta e_m \, . \tag{6-12}$$

By substituting Eqs. (6-11) and (6-12), Eq. (6-10) becomes a set of three linear equations with three unknowns, Δe_a, Δe_b and Δe_c. The solutions are substituted to Eq. (6-12) to determine the new estimate for end-of-time-step temperatures. This procedure is iterated until the convergence criterion,

$$\left|\frac{\Delta e_m}{e_m^k}\right| < \varepsilon \quad , \tag{6-13}$$

is satisfied. The convergence is quick in most cases and several iterations are normally sufficient, as long as an appropriate time-step control is made. Finally the end-of-time-step macroscopic densities are updated straightforward using Eq. (6-8).

6.4. Fission Gas Plenum Heat Transfer

The fission-gas plenum regions can be placed both above and below a pin fuel or

control pellet column. Each region extends over several axial mesh cells, the volume fraction in each cell is defined by the input pin non-flow volume. Fission gas possesses single average temperature and undergoes heat transfer with the cladding, for which axial temperature distribution is defined. The heat-transfer calculation is operated at the same time step as the pin heat transfer. Unlike the pin fuel region, however, the fission gas temperature is updated explicitly, because the thermal response of gas is rather slow due to low thermal conductivity.

When the cladding in the fission-gas plenum region is predicted to fail, the gas space is made available to fluid flow. However, no gas blow-down is modeled in a simplified pin model, and the gas mass is simply neglected.

The mass and energy conservation equations for the cladding and fission gas in a plenum region are expressed as

$$\frac{\partial \overline{\rho}_c}{\partial t} = \Gamma_c \,, \tag{6-14}$$

$$\frac{\partial \overline{\rho}_c e_c}{\partial t} = h_{FG,c} a_{FG,c} \left(T_{FG} - T_c \right) + Q_{Hc} + Q_{Nc} \quad \text{, and} \tag{6-15}$$

$$\frac{\partial m_{FG} e_{FG}}{\partial t} = \sum_j h_{FG,c} a_{FG,c} \left[T_c(j) - T_{FG} \right] V_{ij} \quad , \tag{6-16}$$

where T_{FG} and e_{FG} denote the temperature and specific internal energy of fission gas, respectively, and V_{ij} is the volume of the fluid-dynamic mesh cell. The mass transfer term appears only in Eq. (6-14), since only the cladding is coupled with fluid. No heat transfer nor nuclear heating terms are included in Eq. (6-16), because fission gas in not coupled with fluid nor no nuclear heat source is defined for fission gas component. The mass of plenum fission gas, m_{FG}, is calculated by

$$m_{FG} = \rho_{FG} V_{FG} \quad , \tag{6-17}$$

where the microscopic density of fission gas is given by the EOS routine, depending on gas temperature, and the total volume of gas plenum is determined upon initialization and kept constant during transient.

The above equations are solved explicitly using the beginning-of-time-step

temperatures as follows. No special solution procedure is necessary.

$$\tilde{\bar{\rho}}_c^{n+1} = \bar{\rho}_c^n + \Delta t \Gamma_c \,, \tag{6-18}$$

$$\tilde{e}_c^{n+1} = \frac{\bar{\rho}_c^n e_c^n + \Delta t \left[h_{FG,c} a_{FG,c} \left(T_{FG}^n - T_c^n \right) + Q_{Hc} + Q_{Nc} \right]}{\tilde{\bar{\rho}}_c^{n+1}} \quad \text{, and} \tag{6-19}$$

$$\tilde{e}_{FG}^{n+1} = e_{FG}^n + \Delta t \frac{\sum_j h_{FG,c} a_{FG,c} \left[T_c^n (j) - T_{FG}^n \right] V_{ij}}{m_{FG}} \quad . \tag{6-20}$$

6.5. Heat-Transfer Time-Step Control

In the standard treatment, the fuel-pin heat-transfer time steps are operated consistently with the reactivity time steps when the neutronics model is used. This approach is taken, because the nuclear heating is directly connected to fuel temperature and the resultant fuel temperature has a direct effect on Doppler reactivity feedback. However, as described previously in Section 6.1, the time steps can be made independent of the neutronics optionally.

The fuel pin heat-transfer time steps are controlled, based on the changes in specific internal energies of pin fuel and cladding. In addition, the time steps are controlled, based on the change in power level, as well, because of close relationship between nuclear heating rate and fuel temperature. The control is based on relative changes in energy and power, and is expressed as

$$\Delta t_m^{new} = 0.9 f_m \frac{\tilde{e}_m^{n+1}}{\left| \tilde{e}_m^{n+1} - e_m^n \right|} \Delta t^{old} \quad \text{, and} \tag{6-21}$$

$$\Delta t_p^{new} = 0.9 f_p \frac{P_m^{n+1}}{\left| P_m^{n+1} - P_m^n \right|} \Delta t^{old} \quad , \tag{6-22}$$

where P_m^n denotes the power amplitude. The input adjustment factors, f, are defaulted to 0.5, and smaller values can be used when a tightened control is desirable. The time step sizes are also restricted by the input minimum and maximum values. Further the time step size is restricted not to exceed the previous size, as well. The resultant criterion is defined by

$$\Delta t^{new} = \max\left[\Delta t_{\min}, \min\left(\Delta t_m^{new}, \Delta t_p^{new}, 4\Delta t^{old}, \Delta t_{\max} \right) \right] \quad . \tag{6-23}$$

6.6. Final Operation

As the result of fuel-pin thermal calculation, the specific internal energies of the pin components are updated. The corresponding fluid-dynamics cell variables are also updated to be consistent with the pin model. A call to EOS routines updates: specific volume, temperature and volume fraction of each pin structure component. The total structure-field volume fraction, α_S, is also updated.

The volume fraction of pin fuel changes depending on specific internal energy. The increase in pin fuel volume is accommodated by decreasing the pin non-flow volume $\alpha_{nf,pin}$. As far as $\alpha_{nf,pin}$ is greater than zero, there is no change in the pin volume fraction. When the pin fuel further expands, $\alpha_{nf,pin}$ is set to zero and the pin volume fraction increases. This causes the reduction in flow volume fraction in the mesh cell. It is noted that no axial fuel expansion is modeled currently.

7. Structure Melting and Breakup Model

7.1. Overview of Structure-Related Mass-Transfer Model

Various modes of mass-transfer processes are modeled in SIMMER-III. Non-equilibrium melting/freezing mass transfers occurring at the interfaces between structure surface and fluid are treated in the fluid-dynamics heat and mass transfer model as described in reference 11. This section presents the models for other modes of mass transfer related to the structure. These include equilibrium melting/freezing, solid structure breakup and fission gas release from liquid-field fuel.

All the above operations are included in the fluid-dynamics algorithm and they are not coupled one another. In other words, mass and energy updates are performed in series, each of which deals with a different mass-transfer process. It is noted that the structure breakup mass transfer is calculated at the beginning of the fluid-dynamics algorithm, before the structure configuration is updated, because the breakup transfer instantaneously and drastically changes the structure configuration and the cell hydraulic diameter. The equilibrium melting/freezing transfer is calculated at the end of an intra-cell calculation step, to make sure whether or not the component thermal condition after a series of intra-cell heat-transfer satisfies the phase transition criteria.

7.2. Equilibrium Melting and Freezing

There are two types of melting and freezing mass-transfer processes modeled in SIMMER-III. Non-equilibrium melting/freezing is operated when the condition at an interface of two components satisfies a certain phase-transition criterion. The mass transfer rate is calculated based on the heat balance at the interface, regardless of the component bulk energy. In this context, the process is called as non-equilibrium.

The intra-cell calculation step called “Step 1” transfers consist of structure breakup, nuclear heating, non-equilibrium heat and mass transfer, and can wall heat transfer. As the results of mass and energy updates for these transfer processes, the solid component temperature may be higher than the melting point or the liquid temperature falls below the melting point. Equilibrium melting/freezing is evaluated, at the end of Step 1, when the specific internal energy of a component exceeds certain phase-transition energy. The mass is transferred such that the remaining mass stays exactly at the phase-transition energy. The mass transfer processes include

non-structure components as well, such as equilibrium melting/freezing transfer between liquid fuel and fuel particles.

The equilibrium melting processes of solid components (crust fuel, can wall, fuel particles and steel particles) are evaluated first. Then the resultant liquid state is updated, since a part of solid mass is transferred to liquid. The equilibrium freezing of liquid components (liquid fuel and steel) are finally evaluated. Since the mass transfers of pin fuel/control and cladding are treated by the structure breakup model, no equilibrium melting is modeled.

7.2.1. Equilibrium melting of crust fuel

If the specific internal energy of crust fuel exceeds the solidus energy of fuel, a part of crust fuel mass is transferred to liquid fuel at the liquidus energy such that the remaining mass stays at the solidus energy. For the left crust fuel, mass and energy equations are expressed as

$$\frac{\partial(\overline{\rho}_{s3}+\overline{\rho}_{s4})}{\partial t}=-\Gamma_{S2,L1}^{EQ}, \text{ and} \tag{7-1}$$

$$\frac{\partial(\overline{\rho}_{s3}+\overline{\rho}_{s4})e_{S2}}{\partial t}=-\Gamma_{S2,L1}^{EQ}\max\left[e_{Liq,1}, e_{S2}^{n}\right], \tag{7-2}$$

where the mass-transfer rate due to equilibrium melting is evaluated by

$$\Gamma_{S2,L1}^{EQ}=\min\left[-\frac{(\overline{\rho}_{s3}+\overline{\rho}_{s4})}{\Delta t}\frac{e_{sol,1}-e_{S2}}{h_{f,1}}, \frac{(\overline{\rho}_{s3}+\overline{\rho}_{s4})}{\Delta t}\right]. \tag{7-3}$$

Here, $h_{f,1}$ denotes the latent heat of fusion of fuel. The mass transfer rate is limited to the maximum value of total mass transfer in the time step. This fuel mass transfer is not accompanied by fission gas mass transfer, since no fission gas is contained in crust fuel. The right crust fuel is treated exactly the same.

7.2.2. Equilibrium melting of can wall

If the specific internal energy of the can wall surface exceeds the solidus energy of steel, a part of can wall mass is transferred to liquid steel at the liquidus energy such that the remaining mass stays as a wall at the solidus energy. When the crust fuel is present on the surface of can wall, underlying structure can still melt and transfer mass

through the fuel crust. This behavior seems unphysical, but still is justified if one assumes the fuel crust is leaky.

When a thick can wall is melting in the surface node that was set over to the adjacent cell, the molten mass is transferred in the adjacent cell. This is reasonable. However a thin can wall is melting due to thermal loading from the adjacent cell, the mass transfer takes place only in the present cell. This behavior is unrealistic; however the influence of this inconsistency is still acceptable, because a thin melting can wall disappears sooner or later.

The mass and energy equations for the melting can wall component m are expressed as

$$\frac{\partial \overline{\rho}_{sm}}{\partial t} = -\Gamma^{EQ}_{Sm,L2} \quad \text{, and} \tag{7-4}$$

$$\frac{\partial (\overline{\rho}_{sm} e_{Sm})}{\partial t} = -\Gamma^{EQ}_{Sm,L2} \max\left[e_{Liq,2}, e^{n}_{Sm}\right], \tag{7-5}$$

where the mass-transfer rate due to equilibrium melting is evaluated by

$$\Gamma^{EQ}_{Sm,L2} = \min\left[-\frac{\overline{\rho}_{sm}}{\Delta t}\frac{e_{sol,2} - e_{Sm}}{h_{f,2}}, \frac{\overline{\rho}_{sm}}{\Delta t}\right]. \tag{7-6}$$

Here, $h_{f,2}$ denotes the latent heat of fusion of steel. The mass transfer rate is limited to the maximum value of total mass transfer in the time step.

7.2.3. Equilibrium melting of fuel particles, steel particles and fuel chunks

The modeling concept is similar to the previous cases, and the mass and energy equations for melting fuel or steel particles are written as

$$\frac{\partial \overline{\rho}_{lm}}{\partial t} = -\Gamma^{EQ}_{Lm,L(m-3)} \quad \text{, and} \tag{7-7}$$

$$\frac{\partial (\overline{\rho}_{lm} e_{Lm})}{\partial t} = -\Gamma^{EQ}_{Lm,L(m-3)} \max\left[e_{Liq,(m-3)}, e^{n}_{Lm}\right], \tag{7-8}$$

where $m = 4$ for fuel and $m = 5$ for steel, and the mass-transfer rate due to equilibrium melting is evaluated by

$$\Gamma^{EQ}_{Lm,L(m-3)} = \min\left[-\frac{\overline{\rho}^{n}_{lm}}{\Delta t}\frac{e_{Sol,(m-3)} - e^{n}_{Lm}}{h_{f,m-3}}, \frac{\overline{\rho}^{n}_{lm}}{\Delta t} \right] . \quad (7\text{-}9)$$

Similarly, the mass and energy equations for melting of fuel chunks are given by

$$\frac{\partial(\overline{\rho}_{l9} + \overline{\rho}_{l10})}{\partial t} = -\Gamma^{EQ}_{L7,L1} \quad \text{, and} \quad (7\text{-}10)$$

$$\frac{\partial(\overline{\rho}_{l9} + \overline{\rho}_{l10})e_{L7}}{\partial t} = -\Gamma^{EQ}_{L7,L1} \max\left[e_{Liq,1}, e^{n}_{L7}\right], \quad (7\text{-}11)$$

where the mass-transfer rate due to equilibrium melting is evaluated by

$$\Gamma^{EQ}_{L7,L1} = \min\left[-\frac{(\overline{\rho}^{n}_{l9} + \overline{\rho}^{n}_{l10})}{\Delta t}\frac{e_{Sol,1} - e^{n}_{L7}}{h_{f,1}}, \frac{(\overline{\rho}^{n}_{l9} + \overline{\rho}^{n}_{l10})}{\Delta t} \right] . \quad (7\text{-}12)$$

The mass is transferred such that the specific internal energy of remaining solid particles is solidus. Here, $h_{f.m-3}$ denotes the latent heat of fusion. The mass transfer rate is limited to the maximum value of total mass transfer in the time step. This fuel mass transfer is accompanied by fission gas mass transfer from fuel particles and fuel chunks to liquid fuel. No direct release to the vapor field is modeled. The fission gas mass-transfer rate is determined from

$$\frac{\partial \overline{\rho}_{l12}}{\partial t} = -\Gamma^{EQ}_{l12,l11} \quad , \quad (7\text{-}13)$$

$$\Gamma^{EQ}_{l12,l11} = \Gamma^{EQ}_{L4,L1}\frac{\overline{\rho}^{n}_{l12}}{\overline{\rho}^{n}_{l5} + \overline{\rho}^{n}_{l6}}, \quad (7\text{-}14)$$

$$\frac{\partial \overline{\rho}_{l13}}{\partial t} = -\Gamma^{EQ}_{l13,l11} \quad \text{, and} \quad (7\text{-}15)$$

$$\Gamma^{EQ}_{l13,l11} = \Gamma^{EQ}_{L7,L1}\frac{\overline{\rho}^{n}_{l13}}{\overline{\rho}^{n}_{l9} + \overline{\rho}^{n}_{l10}}, \quad (7\text{-}16)$$

where $\Gamma^{EQ}_{L4,L1}$ and $\Gamma^{EQ}_{L7,L1}$ are the mass transfer rates due to equilibrium melting of fuel particles and fuel chunks as calculated by Eq. (7-9) and (7-12).

7.2.4. Update of liquid state as resulted from equilibrium melting

As the result of equilibrium melting of solid components, the thermodynamic state of

the liquid field is changed. The macroscopic density of a liquid component is simply updated using the mass transfer rate. The specific internal energy of liquid fuel is updated by

$$\frac{\partial(\overline{\rho}_{l1}+\overline{\rho}_{l2})e_{L1}}{\partial t}=\Gamma^{EQ}_{S2,L1}\max\left[e_{Liq,1},e^{n}_{S2}\right]+\Gamma^{EQ}_{S3,L1}\max\left[e_{Liq,1},e^{n}_{S3}\right]$$
$$+\Gamma^{EQ}_{L4,L1}\max\left[e_{Liq,1},e^{n}_{L4}\right]+\Gamma^{EQ}_{L7,L1}\max\left[e_{Liq,1},e^{n}_{L7}\right]\ . \qquad (7\text{-}17)$$

The specific internal energy of liquid steel is updated by

$$\frac{\partial\overline{\rho}_{l3}e_{L2}}{\partial t}=\sum_{m=5}^{8}\Gamma^{EQ}_{Sm,L2}\max\left[e_{Liq,2},e^{n}_{Sm}\right]+\Gamma^{EQ}_{L5,L2}\max\left[e_{Liq,2},e^{n}_{L5}\right]\ . \qquad (7\text{-}18)$$

The macroscopic density of fission gas in liquid fuel is updated by

$$\frac{\partial\overline{\rho}_{l11}}{\partial t}=-\Gamma^{EQ}_{l12,l11}-\Gamma^{EQ}_{l13,l11}\ . \qquad (7\text{-}19)$$

7.2.5. Equilibrium freezing of liquid fuel

The liquid fuel can freeze into either crust fuel or solid fuel particles. The former mode of mass transfer is modeled as non-equilibrium fuel freezing on a structure surface. It is assumed that equilibrium freezing results in formation of solid particles. This mode of fuel freezing is very important, since it describes the so-called bulk freezing mechanism. The mass and energy equations for the solidifying liquid fuel is written as

$$\frac{\partial(\overline{\rho}_{l1}+\overline{\rho}_{l2})}{\partial t}=-\Gamma^{EQ}_{L1,L4}\text{, and} \qquad (7\text{-}20)$$

$$\frac{\partial(\overline{\rho}_{l1}+\overline{\rho}_{l2})e_{L1}}{\partial t}=-\Gamma^{EQ}_{L1,L4}\min\left[e_{Sol,1},e^{n}_{L1}\right]\ , \qquad (7\text{-}21)$$

where the mass-transfer rate due to equilibrium freezing is evaluated by

$$\Gamma^{EQ}_{L1,L4}=\min\left[-\frac{\left(\overline{\rho}^{n}_{l1}+\overline{\rho}^{n}_{l2}\right)}{\Delta t}\frac{e_{Liq,1}-e^{n}_{L1}}{h_{f,1}},\frac{\left(\overline{\rho}^{n}_{l1}+\overline{\rho}^{n}_{l2}\right)}{\Delta t}\right]\ . \qquad (7\text{-}22)$$

The mass is transferred such that the specific internal energy of remaining liquid fuel is liquidus. The macroscopic density and specific internal energy of the solid fuel particles are updated by

$$\frac{\partial(\overline{\rho}_{l5}+\overline{\rho}_{l6})}{\partial t}=\Gamma_{L1,L4}^{EQ}, \text{ and} \tag{7-23}$$

$$\frac{\partial(\overline{\rho}_{l5}+\overline{\rho}_{l6})e_{L4}}{\partial t}=-\Gamma_{L1,L4}^{EQ}\min\left[e_{Sol,1},e_{L4}^{n}\right] . \tag{7-24}$$

This fuel mass transfer is accompanied by fission gas mass transfer from liquid fuel to fuel particles. The fission gas mass-transfer rate is determined similarly to Eqs. (7-13) - (7-16).

7.2.6. Equilibrium freezing of liquid steel

The equilibrium freezing of liquid steel is assumed to result in steel particle formation. The mass and energy equations for freezing liquid steel are written as

$$\frac{\partial\overline{\rho}_{l3}}{\partial t}=-\Gamma_{L2,L5}^{EQ} , \text{ and} \tag{7-25}$$

$$\frac{\partial\overline{\rho}_{l3}e_{L2}}{\partial t}=-\Gamma_{L2,L5}^{EQ}\min\left[e_{Sol,2},e_{L2}^{n}\right] , \tag{7-26}$$

where the mass-transfer rate due to equilibrium freezing is evaluated by

$$\Gamma_{L2,L5}^{EQ}=\min\left[\frac{\overline{\rho}_{l3}^{n}}{\Delta t}\frac{e_{Liq,2}-e_{L2}^{n}}{h_{f,2}},\frac{\overline{\rho}_{l3}^{n}}{\Delta t}\right] . \tag{7-27}$$

The mass is transferred such that the specific internal energy of remaining liquid steel is liquidus. The macroscopic density and specific internal energy of the solid steel particles are updated by

$$\frac{\partial\overline{\rho}_{l7}}{\partial t}=\Gamma_{L2,L5}^{EQ} , \text{ and} \tag{7-28}$$

$$\frac{\partial\overline{\rho}_{l7}e_{L5}}{\partial t}=\Gamma_{L2,L5}^{EQ}\min\left[e_{Sol,2},e_{L2}^{n}\right]. \tag{7-29}$$

The optional paths are considered in which freezing of liquid steel onto cladding and can-wall surfaces. The mass and energy equations for equilibrium freezing of steel are

$$\frac{\partial\overline{\rho}_{l3}}{\partial t}=-\Gamma_{L2,L5}^{EQ}-\Gamma_{L2,S4}^{EQ}-\Gamma_{L2,S5}^{EQ}-\Gamma_{L2,S7}^{EQ} , \tag{7-30}$$

$$\frac{\partial \overline{\rho}_{l7}}{\partial t} = \Gamma^{EQ}_{L2,L5} \quad , \tag{7-31}$$

$$\frac{\partial \overline{\rho}_{Sm}}{\partial t} = \Gamma^{EQ}_{L2,Sm} \quad , \tag{7-32}$$

$$\frac{\partial \overline{\rho}_{l3} e_{L2}}{\partial t} = -\left(\Gamma^{EQ}_{L2,L5} + \Gamma^{EQ}_{L2,S4} + \Gamma^{EQ}_{L2,S5} + \Gamma^{EQ}_{L2,S7}\right) \min\left[e_{Liq,2}, e^n_{L2}\right] \ , \tag{7-33}$$

$$\frac{\partial \overline{\rho}_{l7} e_{L5}}{\partial t} = \Gamma^{EQ}_{L2,L5} \min\left[e_{Sol,2}, e^n_{L5}\right] \ , \text{ and} \tag{7-34}$$

$$\frac{\partial \overline{\rho}_{Sm} e_{Sm}}{\partial t} = \Gamma^{EQ}_{L2,Sm} \min\left[e_{Sol,2}, e^n_{Sm}\right] \ . \tag{7-35}$$

where m=4, 5 and 7 are for cladding, and left and right can-wall surfaces, respectively. The mass-transfer rates due to equilibrium freezing are evaluated by

$$\Gamma^{EQ}_{L2,L5} = \min\left[\frac{\overline{\rho}^n_{l3}}{\Delta t}\left(1 - X_B\right)\frac{e_{Liq,2} - e^n_{L2}}{h_{f,2}}, \frac{\overline{\rho}^n_{l3}}{\Delta t}\left(1 - X_B\right)\right] \ , \text{ and} \tag{7-36}$$

$$\Gamma^{EQ}_{L2,Sm} = \min\left[\frac{\overline{\rho}^n_{l3}}{\Delta t}\frac{e_{Liq,2} - e^n_{L2}}{h_{f,2}}\frac{a_{L2,Sm}}{\sum_m a_{L2,Sm}} X_B, \frac{\overline{\rho}^n_{l3}}{\Delta t}\frac{a_{L2,Sm}}{\sum_m a_{L2,Sm}} X_B\right] \ . \tag{7-37}$$

where X_B stands for the fraction of liquid steel component in the continuous region of liquid steel, and $a_{L2,Sm}$ represents contact areas between the liquid-steel continuous phase and the surfaces of cladding, and left and right can walls (m=4, 5 and 7).

7.3. Fission Gas Release from Liquid Field Components

The behavior of fission gas in the liquid field is treated outsides the scope of structure modeling, but is described here. This is because the fission gas originates from pin fuel and is closely related to the mass transfer of fuel. The fission gas mass transfers associated with equilibrium melting/freezing of fuel are described in the previous section. The release of fission gas in liquid field to the vapor field is described in this section.

The fission gas release from liquid fuel and solid fuel particles is modeled simply by a user-specified release time constants. Typical values for the release time constants

are 10^{-3} and 10^{-1} s for the liquid fuel and solid fuel particles/chunks, respectively. This reflects the general understanding that the fission gas in fully molten fuel is released very quickly, whilst it is released slowly form partially molten fuel. The resultant fission gas release rates are defined by

$$\Gamma_{l11,g5} = -\frac{\partial \overline{\rho}_{l11}}{\partial t} = \min\left[\frac{f_{l11,g5}}{\tau_{l11,g5}} \overline{\rho}^{n}_{l11}, \frac{\overline{\rho}^{n}_{l11}}{\Delta t} \right] \quad , \tag{7-38}$$

$$\Gamma_{l12,g5} = -\frac{\partial \overline{\rho}_{l12}}{\partial t} = \min\left[\frac{f_{l12,g5}}{\tau_{l12,g5}} \overline{\rho}^{n}_{l12}, \frac{\overline{\rho}^{n}_{l12}}{\Delta t} \right] \quad \text{, and,} \tag{7-39}$$

$$\Gamma_{l13,g5} = -\frac{\partial \overline{\rho}_{l13}}{\partial t} = \min\left[\frac{f_{l13,g5}}{\tau_{l13,g5}} \overline{\rho}^{n}_{l13}, \frac{\overline{\rho}^{n}_{l13}}{\Delta t} \right] \quad , \tag{7-40}$$

where $\tau_{l11,g5}$ and $\tau_{l12,g5}$ are the fission gas release time constants, and the rates can be further adjustable by input multipliers, $f_{l11,g5}$ and $f_{l12,g5}$. The macroscopic densities of fission gas in the liquid field are determined by

$$\overline{\rho}^{n+1}_{l11} = \overline{\rho}^{n}_{l11} - \Delta t \Gamma_{l11,g5}, \tag{7-41}$$

$$\overline{\rho}^{n+1}_{l12} = \overline{\rho}^{n}_{l12} - \Delta t \Gamma_{l12,g5} \quad \text{, and} \tag{7-42}$$

$$\overline{\rho}^{n+1}_{l13} = \overline{\rho}^{n}_{l13} - \Delta t \Gamma_{l13,g5} \quad . \tag{7-43}$$

As the result of gas release, the macroscopic density of fission gas in the vapor field is updated by

$$\overline{\rho}^{n+1}_{g5} = \overline{\rho}^{n}_{g5} + \Delta t\left(\Gamma_{l11,g5} + \Gamma_{l12,g5} \Gamma_{l13,g5} \right). \tag{7-44}$$

This changes the vapor state in a mesh cell. Although the internal energy of fission gas in the liquid field is neglected, the gas released to the vapor field needs to carry its energy. Otherwise the resultant specific internal energy of a vapor mixture may be decreased instantaneously. It is therefore assumed that the gas from liquid fuel is at the temperature T_{L1}, the gas from solid fuel particles T_{L4}, and the gas from solid fuel chunks T_{L7}.. Thus the specific internal energy of the vapor mixture is re-defined by

$$e^{n+1}_{G} = \frac{\sum_{m=1}^{4} \left(\overline{\rho}^{n}_{Gm} e^{n}_{Gm} \right) + \Delta t \left[\Gamma_{l11,g5} e_{G4}\left(T_{L1}\right) + \Gamma_{l12,g5} e_{G4}\left(T_{L4}\right) + \Gamma_{l13,g5} e_{G4}\left(T_{L7}\right) \right]}{\sum_{m=1}^{4} \overline{\rho}^{n}_{Gm} + \Delta t \left[\Gamma_{l11,g5} + \Gamma_{l12,g5} + \Gamma_{l13,g5} \right]}, \tag{7-45}$$

where $e_{G4}(T_{L1})$, for example, is the specific internal energy of fission gas at T_{L1} calculated by the EOS model. The vapor temperature is then calculated, by iteratively solving the EOS relationship,

$$\Delta e_G = \frac{\partial e_G}{\partial T_G} \Delta T_G \quad , \tag{7-46}$$

using the Newton-Raphson method with

$$T_G^{k+1} = T_G^k - \frac{e_G\left(T_G^k\right) - e_G^{k+1}}{\left(\frac{\partial e_G}{\partial T_G}\right)} . \tag{7-47}$$

It is noted again that when the fission gas is released to the vapor field, total energy of the system is increased. This simplification, however, does not introduce a energy non-conservation problem, since the internal energy of fission gas is negligibly small in comparison with other liquid and solid components.

7.4. Fuel Pin Breakup

The failure of a fuel pin is modeled only by thermal criteria, in the present simplified pin model. This mode of mass transfer is called as breakup, because mass transfer processes include both melting and solid disintegration. The non-equilibrium heat and mass transfer model allows the cladding surface melting, but the mass transfer at the pin fuel surface is neglected. The equilibrium melting/freezing model (Section 7.2) does not model mass-transfer modes associated with fuel pin or control pin.

In this section, the models are described for fuel and cladding breakup, control breakup and other special modes of fuel breakup. After the heat and mass transfers due to structure breakup are calculated, the structure volume fraction is updated. Since the structure breakup drastically changes the structure volume fraction and the flow configuration, the operations are performed at the beginning of Step 1.

7.4.1. Fuel failure criteria

In the simplified pin model, the criteria to predict failure of pin fuel and cladding are based on melt fractions,

$$\frac{e_p - e_{Sol,1}}{e_{Liq,1} - e_{Sol,1}} \geq f_p^i \quad \text{, and} \tag{7-48}$$

$$\frac{e_c - e_{Sol,2}}{e_{Liq,2} - e_{Sol,2}} \geq f_c^i \quad \text{, respectively,} \tag{7-49}$$

where f_p^i and f_c^i are the input threshold melt fractions, and e_p is the average specific internal energy of pin fuel defined by

$$e_p = \frac{\overline{\rho}_a e_a + \overline{\rho}_b e_b}{\overline{\rho}_a + \overline{\rho}_b} . \tag{7-50}$$

The default values for f_p^i and f_c^i are set to be 0.5 and 0.0, respectively. That is, in the standard treatment, pin fuel breaks up at the mass melt fraction of 50% and cladding breaks up at the solidus energy. Since the above failure prediction is made at the end of each pin heat-transfer time step, the time of failure is predicted only at larger time intervals. This error in failure timing is well acceptable, considering the simplicity of the current pin model. Actual mass transfer operations are preformed in the next fluid-dynamics time step.

7.4.2. Breakup of pin fuel

When the failure criterion is satisfied for pin fuel, the mass transfer is calculated as follows. First the mass transfer due to pin fuel breakup is assumed to occur instantaneously, the macroscopic densities of pin fuel components are set to zero, namely

$$\widetilde{\overline{\rho}}_a^{n+1} = \widetilde{\overline{\rho}}_b^{n+1} = \widetilde{\overline{\rho}}_{\text{int}}^{n+1} = \widetilde{\overline{\rho}}_{s1}^{n+1} = \widetilde{\overline{\rho}}_{s2}^{n+1} = 0 \quad \text{, and} \tag{7-51}$$

$$\widetilde{e}_a^{n+1} = \widetilde{e}_b^{n+1} = \widetilde{e}_{\text{int}}^{n+1} = \widetilde{e}_{S1}^{n+1} = \widetilde{e}_{S,1}^{0} \quad . \tag{7-52}$$

The fuel mass transfer to liquid fuel and solid fuel particles is based on the melt fraction at failure,

$$f_p = \frac{e_p - e_{Sol,1}}{e_{Liq,1} - e_{Sol,1}} \quad . \tag{7-53}$$

The fuel mass is partitioned between fissile and fertile components in liquid field. The specific internal energies are averaged with the existing components. Thus the liquid field is updated as follows:

$$\overline{\rho}_{l1}^{n+1} = \overline{\rho}_{l1}^{n} + \left(\overline{\rho}_a^n + \overline{\rho}_b^n\right) f_p \frac{\overline{\rho}_{s1}^n}{\overline{\rho}_{s1}^n + \overline{\rho}_{s2}^n} , \tag{7-54}$$

$$\overline{\rho}_{l2}^{n+1} = \overline{\rho}_{l2}^{n} + \left(\overline{\rho}_{a}^{n} + \overline{\rho}_{b}^{n}\right) f_p \frac{\overline{\rho}_{s2}^{n}}{\overline{\rho}_{s1}^{n} + \overline{\rho}_{s2}^{n}}, \tag{7-55}$$

$$e_{L1}^{n+1} = \frac{\left(\overline{\rho}_{l1}^{n} + \overline{\rho}_{l2}^{n}\right) e_{L1}^{n} + \left(\overline{\rho}_{a}^{n} + \overline{\rho}_{b}^{n}\right) f_p e_{Liq,1}}{\widetilde{\overline{\rho}}_{l1}^{n+1} + \widetilde{\overline{\rho}}_{l2}^{n+1}}, \tag{7-56}$$

$$\overline{\rho}_{l5}^{n+1} = \overline{\rho}_{l5}^{n} + \left(\overline{\rho}_{a}^{n} + \overline{\rho}_{b}^{n}\right)\left(1 - f_p\right)\frac{\overline{\rho}_{s1}^{n}}{\overline{\rho}_{s1}^{n} + \overline{\rho}_{s2}^{n}}, \tag{7-57}$$

$$\overline{\rho}_{l6}^{n+1} = \overline{\rho}_{l6}^{n} + \left(\overline{\rho}_{a}^{n} + \overline{\rho}_{b}^{n}\right)\left(1 - f_p\right)\frac{\overline{\rho}_{s2}^{n}}{\overline{\rho}_{s1}^{n} + \overline{\rho}_{s2}^{n}} \quad \text{, and} \tag{7-58}$$

$$e_{L4}^{n+1} = \frac{\left(\overline{\rho}_{l5}^{n} + \overline{\rho}_{l6}^{n}\right) e_{L4}^{n} + \left(\overline{\rho}_{a}^{n} + \overline{\rho}_{b}^{n}\right)\left(1 - f_p\right) e_{Sol,1}}{\widetilde{\overline{\rho}}_{l5}^{n+1} + \widetilde{\overline{\rho}}_{l6}^{n+1}} \quad . \tag{7-59}$$

In an optional mass transfer from pin fuel to fuel chunks, the mass and energy of fuel chunks are updated as follows:

$$\widetilde{\overline{\rho}}_{l9}^{n+1} = \overline{\rho}_{l9}^{n} + \left(\overline{\rho}_{a}^{n} + \overline{\rho}_{b}^{n}\right)\left(1 - f_p\right)\frac{\overline{\rho}_{s1}^{n}}{\overline{\rho}_{s1}^{n} + \overline{\rho}_{s2}^{n}}, \tag{7-60}$$

$$\widetilde{\overline{\rho}}_{l10}^{n+1} = \overline{\rho}_{l10}^{n} + \left(\overline{\rho}_{a}^{n} + \overline{\rho}_{b}^{n}\right)\left(1 - f_p\right)\frac{\overline{\rho}_{s2}^{n}}{\overline{\rho}_{s1}^{n} + \overline{\rho}_{s2}^{n}} \quad \text{, and} \tag{7-61}$$

$$\widetilde{e}_{L7}^{n+1} = \frac{\left(\overline{\rho}_{l9}^{n} + \overline{\rho}_{l10}^{n}\right) e_{L7}^{n} + \left(\overline{\rho}_{a}^{n} + \overline{\rho}_{b}^{n}\right)\left(1 - f_p\right) e_{Sol,1}}{\widetilde{\overline{\rho}}_{l9}^{n+1} + \widetilde{\overline{\rho}}_{l10}^{n+1}} \quad . \tag{7-62}$$

The fission gas retained in pin fuel is also transferred to the liquid field, and the mass is partitioned between liquid fuel and solid fuel particles/chunks similarly to fuel transfer:

$$\widetilde{\overline{\rho}}_{l11}^{n+1} = \overline{\rho}_{l11}^{n} + f_p \overline{\rho}_{FG}^{n} \quad , \tag{7-63}$$

$$\widetilde{\overline{\rho}}_{l12}^{n+1} = \overline{\rho}_{l12}^{n} + \left(1 - f_p\right)\overline{\rho}_{FG}^{n} \quad \text{, and} \tag{7-64}$$

$$\widetilde{\overline{\rho}}_{l13}^{n+1} = \overline{\rho}_{l13}^{n} + \left(1 - f_p\right)\overline{\rho}_{FG}^{n} \quad . \tag{7-65}$$

Upon pin fuel breakup, the cladding is also assumed to break up simultaneously. This means the pin fuel breakup represents the condition of total disintegration of fuel pin geometry. In addition, this treatment is necessary to avoid the unphysical situation that the remaining cladding stays intact with no pin fuel inside. This is operated by

$$\tilde{\overline{\rho}}_c^{n+1} = \tilde{\overline{\rho}}_{s7}^{n+1} = 0 \quad , \quad \tilde{e}_c^{n+1} = \tilde{e}_{S4}^{n+1} = e_{S,2}^0 \quad , \tag{7-66}$$

$$\tilde{\overline{\rho}}_{l7}^{n+1} = \overline{\rho}_{l7}^n + \overline{\rho}_{s7}^n \quad \text{, and} \tag{7-67}$$

$$\tilde{e}_{L5}^{n+1} = \frac{\overline{\rho}_{l7}^n e_{L5}^n + \overline{\rho}_{s7}^n e_{S4}^n}{\tilde{\overline{\rho}}_{l7}^{n+1}} \quad . \tag{7-68}$$

7.4.3. Breakup of cladding

When the failure criterion as in Eq. (7-49) is satisfied, the mass transfer is calculated as follows. First a part of cladding mass is transferred to liquid steel at liquidus energy based on the melt fraction.

$$f_c = \frac{e_c - e_{Sol,2}}{e_{Liq,2} - e_{Sol,2}} \quad , \tag{7-69}$$

$$\overline{\rho}_{l3}^{n+1} = \overline{\rho}_{l3}^n + f_c \overline{\rho}_{s7}^n \quad \text{, and,} \tag{7-70}$$

$$\tilde{e}_{L2}^{n+1} = \frac{\overline{\rho}_{l3}^n e_{L2}^n + f_c \overline{\rho}_{s7}^n e_{Liq,2}}{\tilde{\overline{\rho}}_{l3}^{n+1}} \quad . \tag{7-71}$$

Second a remaining mass is transferred depending on the heat flow. When the failure criterion is satisfied due to the heat-transfer from the pin fuel, the remaining mass is transferred to liquid field as steel particles, which is defined by

$$\tilde{\overline{\rho}}_{l7}^{n+1} = \overline{\rho}_{l7}^n + (1 - f_c)\overline{\rho}_{s7}^n \quad \text{, and} \tag{7-72}$$

$$\tilde{e}_{L5}^{n+1} = \frac{\overline{\rho}_{l7}^n e_{L5}^n + (1 - f_c)\overline{\rho}_{s7}^n e_{Sol,2}}{\tilde{\overline{\rho}}_{l7}^{n+1}} \quad . \tag{7-73}$$

When the failure criterion is satisfied due to heat-transfer from the fluid, a part of the remaining mass stays as a cladding at the solidus energy and the other is transferred to liquid field as steel particles, which is defied by

$$\tilde{\overline{\rho}}_{l7}^{n+1} = \overline{\rho}_{l7}^n + (1 - X_{clad})(1 - f_c)\overline{\rho}_{s7}^n \quad , \tag{7-74}$$

$$\tilde{e}_{L5}^{n+1} = \frac{\overline{\rho}_{l7}^n e_{L5}^n + (1 - X_{clad})(1 - f_c)\overline{\rho}_{s7}^n e_{sol,2}}{\tilde{\overline{\rho}}_{l7}^{n+1}} \, , \tag{7-75}$$

$$\tilde{\overline{\rho}}_{s7}^{n+1} = \overline{\rho}_{s7}^n - \tilde{\overline{\rho}}_{l3}^{n+1} - \tilde{\overline{\rho}}_{l7}^{n+1} \quad \text{, and} \tag{7-76}$$

$$\tilde{e}_{S7}^{n+1} = e_{Sol,2} \quad , \tag{7-77}$$

where X_{clad} is an input threshold.

7.4.4. Breakup of control

The control material (B_4C) stays at low temperature during accidents, is unlikely to melt due to nuclear heating. In the current modeling framework of SIMMER-III, decision was made that control is treated only in a solid state, pin control in the structure field and control particles in the liquid field.

In general, control pins are loosely arranged with a large pitch. Thus unclad control pellet column is unlikely to stay intact. Therefore it is assumed that the control breaks up when cladding is lost. The mass and energy transfers due to control breakup are calculated by

$$\tilde{\overline{\rho}}_a^{n+1} = \tilde{\overline{\rho}}_b^{n+1} = \tilde{\overline{\rho}}_{\mathrm{int}}^{n+1} = \tilde{\overline{\rho}}_{s12}^{n+1} = 0\,,\quad \tilde{e}_a^{n+1} = \tilde{e}_b^{n+1} = \tilde{e}_{\mathrm{int}}^{n+1} = \tilde{e}_{S9}^{n+1} = e_{S,1}^{0}\quad, \tag{7-78}$$

$$\tilde{\overline{\rho}}_{l8}^{n+1} = \overline{\rho}_{l8}^{n} + \overline{\rho}_{s12}^{n}\quad \text{, and} \tag{7-79}$$

$$\tilde{e}_{L6}^{n+1} = \frac{\overline{\rho}_{l8}^{n} e_{L6}^{n} + \overline{\rho}_{s12}^{n} e_{S9}^{n} + \overline{\rho}_{\mathrm{int}}^{n} e_{\mathrm{int}}^{n}}{\tilde{\overline{\rho}}_{l8}^{n+1}}\,. \tag{7-80}$$

7.4.5. Collapse of unsupported pin fuel

A fuel pellet column stays intact even after the cladding melting and relocation, because a narrow pin-bundle configuration can prevent the unclad pellet columns from collapsing in a subassembly dust wall. However, such a situation is considered very unstable mechanically. Also there can be an unphysical situation that upper-core unclad pellets stay in place with no support from below after the lower pin structure breaks up.

For these reasons, a special fuel breakup model is implemented to simulate the collapse of a pellet column or the downfall of unsupported pellets. In this model, it is assumed that a fuel pellet column loses it mechanical integrity if one of the following conditions is satisfied:

(1) Cladding is lost, and subassembly can wall is lost (collapse of pellet column), and

(2) Cladding is lost, and the pin structure in the lower cell is lost (downfall of pellets).

In either case, the result is the instantaneous breakup of pin fuel. The mass and energy transfer due to breakup is calculated similarly to the previous cases, and hence the formulation is not repeated.

7.5. Can Wall and Crust Breakup

7.5.1. Breakup of can wall

The criterion to predict break-up of can wall is based on the melt fraction of can wall interior node,

$$\frac{e_{Sm} - e_{sol,2}}{e_{liq,2} - e_{sol,2}} \geq f_{CW}^{i} \quad (m=6 \text{ or } 8), \tag{7-81}$$

where f_{CW}^{i} is an input threshold.

A part of can-wall mass is transferred to liquid steel at the liquidus energy as follows:

$$f_{CW} = \frac{e_{Sm} - e_{sol,2}}{e_{liq,2} - e_{sol,2}} \quad , \tag{7-82}$$

$$\overline{\rho}_{l3}^{n+1} = \overline{\rho}_{l3}^{n} + f_{CW}\overline{\rho}_{sm}^{n} \quad \text{, and} \tag{7-83}$$

$$e_{L2}^{n+1} = \frac{\overline{\rho}_{l3}^{n} e_{L2}^{n} + f_{CW}\overline{\rho}_{sm}^{n} e_{Liq,2}}{\overline{\rho}_{l3}^{n+1}} \quad . \tag{7-84}$$

A part of remaining mass stays as a wall at the solidus energy and the other part is released to liquid field as steel particles. That is

$$\widetilde{\overline{\rho}}_{l7}^{n+1} = \overline{\rho}_{l7}^{n} + (1 - f_{CW})(1 - X_{CW})\overline{\rho}_{sm}^{n} \quad , \tag{7-85}$$

$$\widetilde{e}_{L5}^{n+1} = \frac{\overline{\rho}_{l7}^{n} e_{L5}^{n} + (1 - f_{c})(1 - X_{CW})\overline{\rho}_{sm}^{n} e_{sol,2}}{\widetilde{\overline{\rho}}_{l7}^{n+1}} \quad , \tag{7-86}$$

$$\widetilde{\overline{\rho}}_{sm}^{n+1} = \overline{\rho}_{sm}^{n} - \widetilde{\overline{\rho}}_{l3}^{n+1} - \widetilde{\overline{\rho}}_{l7}^{n+1} , \tag{7-87}$$

$$\widetilde{e}_{Sm}^{n+1} = e_{Sol,2} , \tag{7-88}$$

where X_{CW} is an input parameter that the can-wall fraction being left as a wall at the thermal breakup.

Break-up of the interior node allows a radial fluid motion under a certain failure hole which gives a pressure loss. Thus, an orifice coefficient for the radial motion is

defined by

$$\beta = \beta_{CW} + f_{CW}(1-\beta_{CW}) \text{ ,and} \tag{7-89}$$

$$C_{ORF} = 1.35(1-\beta)(1-\beta^2)\frac{1}{\beta^2} \text{ ,} \tag{7-90}$$

where β_{CW} is a fractional area of can-wall surface allowing radial fluid motion across the wall. The default value is 0.1.

From the mechanical stability of a can wall structure, it is considered reasonable to implement additional structure breakup mechanisms. When the can wall becomes extremely thin as a result of melting or the temperature of the interior node exceeds a point which the stainless steel looses the stress intensity, the structure integrity can no longer be maintained. Thus, the breakup of can wall is assumed when the thickness falls the condition below,

$$W_{CW} < W_{CW,\min} \text{ ,} \tag{7-91}$$

where $W_{CW,\min}$ is an input threshold of minimum can-wall thickness.

Furthermore, the structure strength significantly decreases as the bulk temperature becomes close to the melting point. Under such a high temperature, it is considered to be reasonable that the breakable structure enables fluids to radially move through a small hole which is assumed to be formed by the partial can-wall failure. Here its failure mechanism is introduced by the condition that the can-wall interior temperature exceeds the following criterion T_{fail} :

$$T_{Sm} > T_{fail} \text{ ,} \tag{7-92}$$

Only the radial motion is allowed in these additional cases as in Eqs. (7-89) and (7-90), and the can wall mass is not transferred to the fluid until the thermal break-up condition of Eq. (7-81) is satisfied.

7.5.2. Breakup of crust fuel

Since the fuel crust itself is thought to be very brittle and fragile, it is assumed that it can stay on a structure wall surface only when underlying structure is intact. Namely, if the can wall disappears or undergoes extensive melting on surface, the fuel

crust is likely to fail. Thus, the breakup of crust fuel is assumed when one of the following two conditions is satisfied.

First, the crust fuel breaks up, when the can wall disappears. For the left crust, the criterion is

$$\overline{\rho}_{s8} + \overline{\rho}_{s9} = 0 \quad . \tag{7-93}$$

Second, the crust fuel becomes unstable, when the underlying wall surface starts to melt. However it is also assumed a thick crust can stay intact even when the underlying structure starts to melt. Thus the crust fuel breakup is judged, for the left crust case, by

$$T_{S5} \geq T_{Sol,2} \quad \text{, and} \tag{7-94}$$

$$W_{CF} < W_{CF,\min} \quad , \tag{7-95}$$

where $W_{CF,\min}$ is an input minimum crust fuel thickness.

The mass and energy of the left crust fuel are transferred to solid fuel particles as follows:

$$\widetilde{\overline{\rho}}_{s3}^{n+1} = \widetilde{\overline{\rho}}_{s4}^{n+1} = 0 \quad , \tag{7-96}$$

$$\widetilde{e}_{S2}^{n+1} = e_{S,1}^{0} \quad , \tag{7-97}$$

$$\widetilde{\overline{\rho}}_{l5}^{n+1} = \overline{\rho}_{l5}^{n} + \overline{\rho}_{s3}^{n} \quad , \tag{7-98}$$

$$\widetilde{\overline{\rho}}_{l6}^{n+1} = \overline{\rho}_{l6}^{n} + \overline{\rho}_{s4}^{n} \quad \text{, and} \tag{7-99}$$

$$\widetilde{e}_{L4}^{n+1} = \frac{\left(\overline{\rho}_{l5}^{n} + \overline{\rho}_{l6}^{n}\right) e_{L4}^{n} + \left(\overline{\rho}_{s3}^{n} + \overline{\rho}_{s4}^{n}\right) e_{S2}^{n}}{\widetilde{\overline{\rho}}_{l5}^{n+1} + \widetilde{\overline{\rho}}_{l6}^{n+1}} \quad . \tag{7-100}$$

The right crust fuel is treated exactly the same.

8. Concluding Remarks

Modeling to treat core structures under the CDA condition is described in the present report. The structure model in SIMMER-III, consisting of fuel pins and subassembly can walls, is modeled to exchange heat and mass with multiphase multicomponent flow and to provide a flow channel for fluid. Furthermore, the structure model is intended for reasonable simulation of core melt-out behavior during CDAs. The model also can represent various structure walls in experimental analyses for the code assessment studies. Therefore, the present structure model alleviates some of limitations in the previous SIMMER-II code. It is expected, therefore, that the future research with SIMMER-III will significantly improve the reliability and accuracy of LMFR safety analysis.

Acknowledgements

The initial stage of this study was jointly performed under the agreement between the United States Nuclear Regulatory Commission and the Power Reactor and Nuclear Fuel Development Corporation, presently called Cycle Development Institute (JNC). The authors are grateful to W. R. Bohl of the Los Alamos National Laboratory for his significant contribution to forming the basis of SIMMER-III. The authors would like to acknowledge K. Morita (presently with Kyushu University) for his effort in the early phase of the model development. Our special thanks are due to M. Sugaya of NESI Inc., F. Inoue and N. Nemura formerly at JNC in programming and debugging, and computational assistance. At the end, thanks are due to H. Yamano and Y. Tobita for reading the draft of the present report and marking a number of helpful suggestions.

References

1 Sa. Kondo, et al., “Integrated Analysis of In-Vessel and Ex-Vessel Severe-Accident Sequences,” Proc. Int. Fast Reactor Safety Mtg., Snowbird, Utah, USA, August 12-16, 1990.

2 N. Nonaka, et al., “Characterization of LMFBR Sever Accident Progression,” Proc. Int. Conf. on Design and Safety of Advanced Nuclear Power Plants (ANP’92), Tokyo, Japan, October 25-29, 1992.

3 W. R. Bohl and L. B. Luck, “SIMMER-II: A Computer Program for LMFBR Disrupted Core Analysis,” LA-11415-MS, Los Alamos National Laboratory Report, June 1990.

4 L. L. Smith, et al., “The SIMMER Program: Its Accomplishment,” Proc. Int. Top. Mtg. on Fast Reactor Safety, Knoxville, Tennessee, USA, April 21-25, 1985.

5 A. M. Tentner, et al., “The SAS4A LMFBR Whole Core Accident Analysis Code,” Proc. Int. Mtg. on Fast Reactor Safety, Knoxville, Tennessee, Vol. 2, p. 998 (1985).

6 H. Yamano, et al., “SIMMER-III: A Computer Program for LMFR Core Disruptive Accident Analysis, Version 3.A Model Summary and Program Description,” JNC Report, JNC TN9400 2003-071, August 2003.

7 Sa. Kondo, et al., “PHASE 2 CODE ASSESSMENT OF SIMMER-III, A COMPUTER PROGRAM FOR LMFR CORE DISRUPTIVE ACCIDENT ANALYSIS,” JNC Report, JNC TN9400 2000-105, September, 2000.

8 H. Yamano, et al., “SIMMER-IV: A Three-Dimensional Computer Program for LMFR Core Disruptive Accident Analysis, Version 2.A Model Summary and Program Description,” JNC Report, JNC TN9400 2003-070, August 2003.

9 K. Morita, et. al., “SIMMER-III Analytic Equation-of-State Model,” JNC Report, JNC TN9400 2000-005 (May, 1999).

10 K. Morita, et. al., “Thermodynamic properties and equation of state for fast reactor safety analysis -Part II: Properties of fast reactor materials-,” Nuclear Engineering and Design 183 (1998) pp193-211.

11 K. Morita, et. al., “SIMMER-III Heat- and Mass-Transfer Model –Model and Method Description-," JNC Report, JNC TN9400 2001-074 (August, 2001).